Characterisation of a gun recoil resistance model for use in internal ballistic modelling

Riyadh Abdulrahman A Bin Hussain

orcid.org/0000-0003-0903-9959

Dissertation accepted in fulfilment of the requirements for the degree *Master of Science in Engineering Sciences with Mechanical Engineering* at the North-West University

Supervisor: Prof Willem L den Heijer

Co-supervisor: Mr Jaco Bean

Graduation: June 2021

Student number: 27416399

ACKNOWLEDGEMENTS

The successful completion of this study needed a lot of guidance and help from several people to whom I am extremely thankful. The study would not have been successfully completed without the help and contribution of these people. I would like to express my sincere gratitude to Professor Willem L den Heijer, who guided me throughout the study, and my co-supervisor, Jaco Bean, who encouraged and helped me in understanding the critical elements of the study.

I would also like to thank my colleagues at Military Industries Corporation (MIC) for their cooperation, assistance and support whenever I needed them. They helped and inspired me throughout the study and acted as a constant support structure. Furthermore, I would like to thank all the members of MIC for providing the desired scope and opportunity to develop my career by gathering vast amounts of knowledge on the study subject.

I must also give thanks to the research and development team at Rheinmetall Denel Munition (Pty) Ltd (RDM) for their kind and valuable support. They provided the opportunity to enhance my skills and knowledge.

Finally, I would like to express my deepest gratitude to my parents and siblings for the love and support they have shown. My father and mother have supported me every step of my life with their kind and valuable suggestions. Without their love and support, it would not have been possible to come this far. Thank you to all, with love and respect.

ABSTRACT

While ballistics focus on the behaviour of propellant and projectiles, gun mechanics covers the behaviour of all weapon components and mounts under launch conditions. Gun mechanics deals with the stress and strain of the associated system and components, as well as the dynamic behaviour involved. In the design of munitions, understanding the link between the munition and weapon system and the effect they have on each other is critical. Gun recoil is one of these links.

Operational requirements often dictate weapon mass and dimensions, especially when it comes to larger calibre munitions. Fundamentally, this has significant effects on the momentum balance between the projectile and recoiling parts. It influences the ballistic performance of the system, specifically muzzle velocity through recoil. Accurate representations of weapon systems and the ability to model these systems are of critical importance to reduce development time and increase system accuracies.

This research presents a procedure to identify and characterise a gun recoil resistance model based on a single degree of freedom, mass-spring arrangement. The purpose of such a procedure is to serve as a tool to the systems engineer to identify the recoil model that can be used to predict and determine the ballistic effects of gun recoil on munitions.

A fourth-order Runge-Kutta integration is used to numerically predict the spring stiffness of the weapon system. The procedure iterates with a change in equivalent stiffness until convergence between simulated and measured recoil displacement is achieved, using the breech pressure of the weapon system, weapon mass and weapon displacement as inputs.

KEYWORDS: Internal ballistic, muzzle velocity, recoil simulation program, 40 mm proof weapon system, STANAG 4367, recoil system.

LIST OF ABBREVIATIONS

AGL	Automatic grenade launchers
AMC	United States Army Materiel Command
DND	Department of National Defence Canada
DOD	United States Department of Defence
EPVAT	Electronic pressure, velocity and action time
FBD	Free body diagram
fps	Frames per second
HSV	High-speed video
HV	High velocity
IB	Internal ballistic
kHz	Kilohertz
kg	Kilograms
LVDT	Linear variable displacement transducer
MIC	Military Industries Corporation
mm	Millimetres
MPa	Megapascal
m/s	Meter per second
MV	Muzzle velocity
NATO	North Atlantic Treaty Organization
N	Newton
N/m	Newton per meter
Ns	Newton/second
R^2	Correlation coefficient
RDM	Rheinmetall Denel Munition (Pty) Ltd
s	Second
SDOF	Single degree of freedom
STANAG	Standardization agreement

USMA	United States Military Academy

LIST OF SYMBOLS

a	Acceleration
F	Force
F_0	Amplitude of the driving force
$\sum F$	External forces
$\sum F_i$	Impulsive forces due to all external forces
f	Applied force
i	Body
K	Recoil force
k	Stiffness
kx	Spring force
m	Mass
m_i	Mass of the body
m_r	Total mass of recoiling parts
m_{rp}	Mass of recoiling parts
m_c	Mass of propelling charge
m_p	Mass of projectile
p	Linear momentum
p_p	Momentum of projectile
p_c	Momentum of propellant
p_r	Momentum of gun
RR	Resistive recoil force model
t	Time
t_r	Recoiling time
t_{r0}	Beginning of recoiling motion
v	Velocity
v_c	Propellant gas flow velocity

v_i	Velocity of the body
v_p	Muzzle velocity of projectile
v_r	Velocity of recoiling mass
V_{total}	The total volume of material contributing to mass
X	Maximum amplitude of a particular solution
x	Displacement
$\dot{x}$	Velocity
$\ddot{x}$	Acceleration
x_h	Homogeneous solution
x_p	Harmonic response displacement
x_0	Displacement initial condition
$\dot{x}_0$	Velocity initial condition
ω	Frequency
ω_n	Natural frequency of system
ρ	Uniform material density

TABLE OF CONTENTS

LIST OF TABLES

LIST OF FIGURES

CHAPTER 1 - INTRODUCTION

1.1 Background

The study of ballistics can be divided into four major disciplines, internal ballistics, external ballistics, intermediate ballistics, and terminal ballistics. Internal ballistics focuses on the behaviour of the gun, propelling charge, and projectile from ignition of the propelling charge until the projectile exits the gun muzzle. Intermediate ballistics focuses on the behaviour of the projectile during the initial motion as it exits the muzzle. External ballistics, conversely, focuses on the dynamic behaviour of the projectile from muzzle exit until impact. Terminal ballistics covers all the aspects after the projectile hits the target (Carlucci & Jacobson, 2013). This research will focus only on the internal ballistic discipline whilst external, intermediate and terminal ballistics will be ignored. Two types of propulsion mechanisms of the internal ballistic cycle exist: tube-launched and rocket-motor driven. This study focusses only on tube-launched systems.

1.1.1 Tube launch internal ballistic concepts

A tube-launched weapon system can be defined as a projectile launching device containing a projectile guiding tube that is associated with a combustion chamber. The combustion of propellant, which starts in the combustion chamber, propagates hot, high-pressure gasses which propel the projectile through the tube. The muzzle velocity (MV) is the velocity at which the projectile exits the muzzle of the tube and has a direct impact on the range attained by the projectile. MV is considered to be the highest velocity of the projectile (Agrawal, 2010).

Tube launchers

The common term ‘barrel’ is used throughout this study to describe a tube launcher. Barrels are particularly related to rifles, handguns and light calibre weapons, while tubes refer to mortars and large calibre weapons, in which the tube is a part of the barrel. Although the barrels and tubes from which projectiles are propelled come in different shapes and sizes (AMC, 1964), there are two distinct groups: rifled and smooth, as illustrated in Figure 1-1.

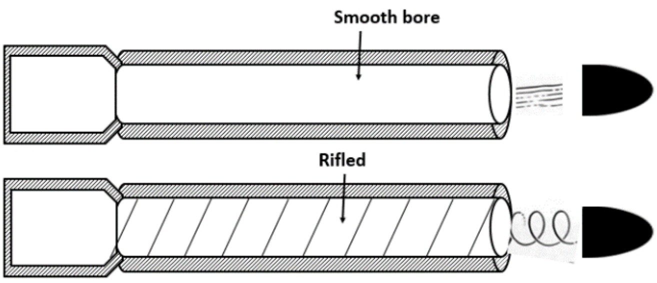

Figure 1-1: Rifled and smooth bore barrel

The U.S. Army Materiel Command (1964) distinguished four main categories of tube-launched weapon systems:

- Larger calibre naval, field and tank guns;
- Small arms and light automatic weapons;
- Mortar launchers; and
- Recoilless guns.

There are specific variations in each of the tube launcher categories with respect to their internal ballistics' parameters. Examples of these are propellant mass, pressure, the type of propellant and characteristics of the propellant (AMC, 1964).

For a firing cycle, the rear end of a tube launcher is closed using a breech to form a combustion chamber, in which the propellant burns to create gas. The discharge end of the tube is referred to as the muzzle. The bore signifies the internal cylindrical space of the tube / barrel. As illustrated in Figure 1-2, the bore is considered to be the central cavity through which the projectile moves (AMC, 1964).

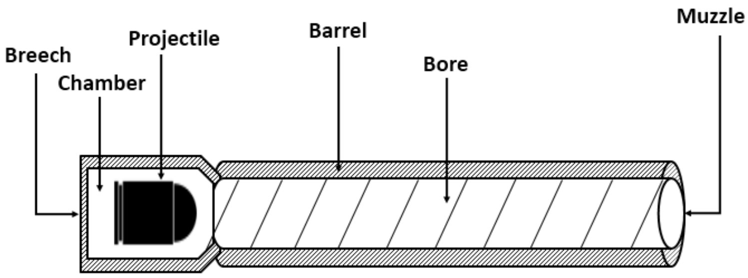

Figure 1-2: General gun barrel construction

1.1.2 Open and closed breech firing

For 'closed breech weapons', the breech is sealed and locked before activating the trigger to fire every shot. This configuration is used in weapons like bolt action rifles, semi-automatic weapons and breech load guns. During the firing cycle, the breech creates a barrier or seal for the tube so that the propellant gas cannot escape the chamber.

For 'open breech weapons', the next round that is going to be fired is loaded in the breech, chambered and fired, just like it is done in automatic weapons. The breech is then moved back by the recoil or gas blowback, the fired / spent cartridge case is ejected, and a subsequent round is then advanced onto the breech for firing. Open breech weapons consume ammunition with the propellant within a cartridge case, resulting in the barrier / seal for the internal ballistic gasses created by the expansion and sealing of the cartridge case against the chamber wall (AMC, 1964). A standard firing cycle is discussed in the following section.

1.1.3 Firing cycle

The series of events that takes place inside the tube when firing a gun can be explained as follows:

1. First, the primer is struck by the firing pin, which causes the ignition to start. Initially, the combustion chamber is at low pressure, and the ignited propellant gradually burns, converting chemical energy into heat and gas (DND Canada, 1992).

2. Next, the gas pressure in the chamber (the space behind the projectile base) increases. This increase is due to the gas from the surface of individual pieces of propellant, creating an increase in the burning rate as well as a rapid accumulation of gas (DND Canada, 1992).

3. Enough pressure builds up to overcome the driving band engraving resistance, thereby accelerating the projectile rapidly down the bore. As a result, the volume of the chamber behind the projectile increases, which decreases the rate at which pressure is increasing. As there is a gradual decrease in pressure, there is a rapid increase in the chamber volume, and the gas consistently evolves until all propellant has been burnt. ‘Propellant of all-burnt’ is the point of the projectile within the barrel where the propellant has been fully consumed, and gas does not evolve further (DND Canada, 1992).

4. When the projectile base clears the muzzle, hot gas is released under extremely high temperature and pressure. This release results in a muzzle flash and burst, along with the characteristically deafening sound of gunfire (DND Canada, 1992).

During the firing process, an enormous force caused by the propellant combustion drives the projectile forward and the gun system in the opposite direction. The motion of the launcher in the opposite direction of the projectile is known as ‘recoil’. A recoil system is integrated into the weapon system to regulate and confine the movement of a recoiling mass during the firing cycle and when the firing cycle is completed (Horn & Boutteville, 1982).

Figure 1-3 illustrates the pressure curve of a projectile travelling down the tube. The pressure rises to a maximum and then falls off until the propellant is all burnt, and the projectile ultimately leaves the tube.

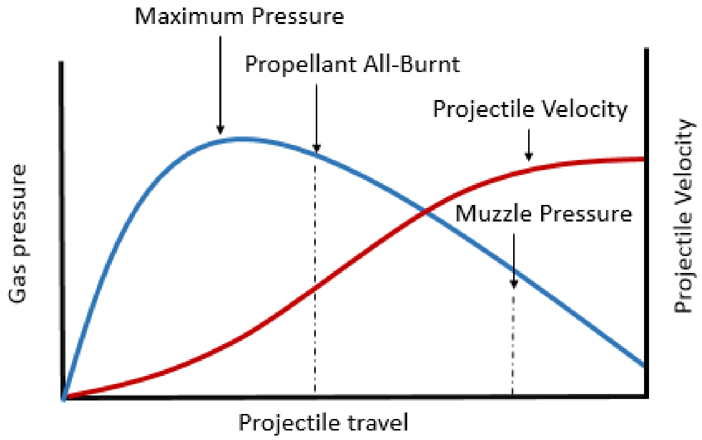

Figure 1-3: Gun chamber pressure and projectile velocity vs projectile displacement

1.1.4 Managing the recoil

Three different types of recoiling configurations are used to manage weapon recoil:

- Free (infinite) recoil;
- Fixed (no) recoil; or
- Limited (finite) recoil.

With free recoil, no constraint (mount points) hold the barrel. Consequently, no forces can be transmitted to the support points.

Fixed recoil is the opposite of the free recoil and, as suggested by its title, indicates that the gun tube remains stationary, incapable of moving under the force from the applied gas pressure. This configuration refers to a rigid structure that transfers the full weapon recoil momentum to the mounts / constraints. The movement of the gun tube is nil. As such, all the necessary force is transferred into accelerating the projectile. This configuration acquires higher muzzle velocities but produces a significantly higher force on the mounts used to hold the gun barrel in place.

The last configuration, limited recoil, is in-between fixed and free recoil in the sense that the gun tube is only allowed to recoil a limited or finite distance (Horn & Boutteville, 1982).

Each of these recoiling configurations has a different influence on the internal ballistics and ultimately, the muzzle velocity of a projectile (Horn & Boutteville, 1982). The relationship between recoil and muzzle velocity is expected because the conservation of momentum ultimately governs it.

1.1.5 Recoil affecting system performance

The momentum within a weapon system during weapon firing is equal and opposite to the momentum imparted to the projectile launched from the weapon and that of propellant gasses subsequently ejected from the weapon system. A recoil force is caused during and after the firing of weapons. However, this recoil force severely affects the performance of any weapon system due to the fact of a counterforce which balances the actual force exerted on the projectile. To illustrate this, Table 1-1 lists the effect of recoil on muzzle velocity for three different weapon systems: 155 mm artillery, 40 mm grenade and 81 mm mortar. The results suggest that, by merely changing from the free recoil to fixed recoil, the muzzle velocity increases. Keeping in mind that muzzle velocity is a direct indicator of the range that will be achieved by a projectile, the recoil configuration consequently influences the range achieved by the projectile. The data presented in Table 1-1 were generated by an internal ballistic simulation program developed and maintained by Rheinmetall Denel Munition (Pty) Ltd (RDM). A 5% change in muzzle velocity for an 81 mm mortar and 1% for a 155 mm artillery typically relates to a change in range of approximately 390 m on a nominal range of 6.1 km (6.3%) and approximately 566 m on a nominal range of 31 km (1.8%), respectively. Although the total effect of recoil (free vs fixed) is negligible for 155 mm artillery, it plays a considerable role in the case of the 81 mm mortar. Therefore, recoil could negatively affect the dispersion performance of the mortar, and in severe cases, cause unintentional target hits or mission failures.

Table 1-1: The influence of fixed and free recoil on MV

Different Systems / Performance Parameter	155 mm artillery	40 mm grenade	81 mm mortar
Muzzle velocity difference	1.01 %	1.93 %	5.17 %
Projectile muzzle velocity (free recoil) (m/s)	942.93	121.90	299.23
Projectile muzzle velocity (no recoil) (m/s)	952.47	124.31	315.54

1.1.6 How a recoil system is modelled

Current literature mostly studies the linear approximation of the recoil resistance. This linear resistance model, introduced in detail throughout Chapter 2, is often used as a tool to calibrate internal ballistic models with experimental results. The STANAG 4367 manual for instance, makes use of a recoil resistance model, as illustrated in Figure 1-4, which is notably generalised and changes when applied to various systems. The characteristics of this model are also changed as a way of calibrating the internal ballistic model with experimental results. This model is the most commonly accepted model in use, and not many alternative recoil resistance models exist.

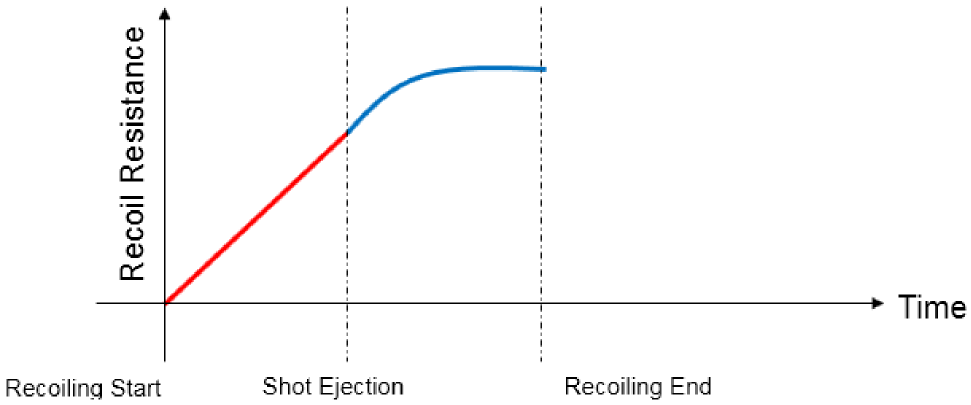

Figure 1-4: Common recoil resistance models (STANAG 4367)

Scope exists for developing a process of identifying an accurate model that describes recoiling motion and recoil resistance of a gun system, considering the effect of recoil on the system performance Section 1.1.5 and the limited modelling techniques and literature available on recoil modelling Section 1.1.6. This model will allow internal ballisticians to optimise internal ballistic calculations and predictions.

1.2 Problem Statement

The recoil can negatively impact the performance of the ballistic system, as mentioned in section 1.1.5. However, the characteristics of the recoil system usually are classified by their producers. As a consequence, it is vital to develop a framework to characterise the recoil system. Then, these characteristics can be used in the internal ballistic modelling to improve the simulation programme accuracy.

1.3 Objectives

The objectives of the research is to develop a framework to characterise any recoil system (spring only). In addition to that, it is to generate these characteristics to be used in internal ballistic modelling to improve the simulation programme accuracy.

1.4 Research methodology

- Derivation of a system model

  A numerical model based on a single degree of freedom (SDOF) mass-spring arrangement will be derived in the computer software package MATLAB. The model should be capable of identifying the equivalent linear system spring stiffness using experimental data (breech pressure, weapon mass and weapon displacement) as inputs.

  An analytical SDOF model, with known mass and spring stiffness, will be used to generate an excitation force and displacement data (similar to that gathered during experimental trials). The generated data will then be used as inputs to the numerical model to verify if the numerical model converges to the same spring stiffness used to generate the data.

- Experimental measurements

  A series of 40 mm rounds will be fired while measuring the breech pressure, recoil displacement, muzzle velocity and acceleration.

- Characterisation of a system model

  The derived simulation model will be used to predict the equivalent spring stiffness of the weapon system using the data gathered from experimental measurements.

- Characterisation of system spring stiffness

  The equivalent spring stiffness of the weapon system will be identified using a load cell and displacement transducer. The experimentally identified spring stiffness will then be compared to the predicted spring stiffness (of the previous objective) as experimentally characterised to validate the numerical model.

1.5 Limitations of the Study

- The process of identifying the recoil resistance model is demonstrated for a specific weapon system (40 mm) only, comprising an equivalent linear spring stiffness recoil element.
- Only linear spring stiffness was considered in this study.
- The characterisation of damping of the recoil model is not part of this study.
- The inherent damping in the weapon (stemming from the friction of bearings, friction between the guide rods and sliding bushes of the recoiling jig / platform and elastic deformation of the weapon and recoiling parts) is not part of this study.
- The budget dedicated to this research is extremely limited.
- The access to the RDM's test range, measuring equipment, and data are extremely restricted.

1.6 Contributions of the Study

This research will:

- Identify a recoil resistance model to be used in internal ballistic calculations.
- Provide deeper understanding of the recoiling behaviour and its effect on internal ballistics.
- Present a structured procedure to characterise recoil model and to be used by internal ballisticians.

1.7 Summary

This chapter provided the background of the research, explained the research problem statement and described the research objectives. This chapter further described the research limitations and listed the study contributions.

The chapter that follow reviews the literature that supports the research.

CHAPTER 2 - LITERATURE STUDY

2.1 Introduction

This chapter introduces recoil systems and their role in a ballistic system by investigating subsystems and the forces that drive recoil. The concept of internal ballistic modelling, the functions of the recoil system and components of a recoil mechanism are also discussed. This chapter introduces the background of vibrations in a relatively simple manner, including the mass-spring vibrating system and free vibration of SDOF systems. The chapter concludes with a review of the resistive recoil force model, concept of impulse and momentum for a gun system.

2.2 Internal Ballistic Modelling Concept

The internal ballistic model contains several sub-models. The purpose of such a model is to calculate the entire internal ballistic cycle in a gun (as discussed in Section 1.4) and generate valuable predictions, such as the muzzle velocity and the maximum chamber pressure of a ballistic system. The internal ballistic model aids the propelling charge designer to develop new propelling charge systems, improve and analyse existing systems, perform generic support and investigative prediction or analysis (Carlucci & Jacobson, 2013). It also allows internal ballisticians to determine the proper charge mass to keep the muzzle velocity within the allowable error margin.

A typical scenario is presented below, generated by an internal ballistic simulation program used at RDM. It summarises the effect of recoil on muzzle velocity for 60 mm weapon systems. The 60 mm projectile has a muzzle velocity of 310 ± 3 m/s as specified by the company's standards. However, the fixed recoil MV is 315 m/s and the free recoil MV is 299 m/s. The recoil effect of the recoil can be calculated by subtracting the two MVs; thus, it will be 16 m/s. Note that the recoil effect on MV exceeded the tolerance of the projectile MV. The maximum effect of gun recoil can be as high as 16 m/s. This effect will severely affect the projectile MV tolerance (3 m/s), and therefore recoiling should be considered when developing ammunition or charges (Schabort, 2016).

2.3 The Role of Recoil

The force impulse magnitude acting on the breech is increased as the breech pressure increases. The force acting on the breech is considered as the input load to the recoil system. The recoil system converts the high amplitude breech force impulse and increases the duration of the impulse while reducing the amplitude of the impulse. The lower-amplitude, longer-duration impulse is considered to be the recoil system output. Figure 2-1 below illustrates the concepts of the input force and output force of a recoil system. As can be seen, the input force curve has a higher amplitude and shorter duration and represents the force on the breech. The output force curve has a lower amplitude and longer duration and represents the recoil system's reaction to the input force (USMA, 1980).

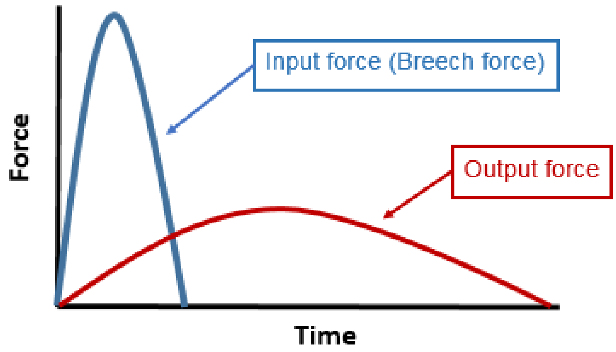

Figure 2-1: Two recoil forces having the same total force size

2.4 Functions of Recoil Systems

The recoil mechanism essentially seeks to convert extremely large internal ballistic forces acting on the recoiling parts to tolerable forces that are acting on the supporting structure. The enormous internal ballistic force (breech force) that is acting on the recoiling parts, represented by $F(t)$ in Figure 2-2, acts in less than 0.005 s for 40 mm guns (Gander, 2002). These extensive forces accelerate the lightweight projectile out of the bore at very high velocities. The heavy recoiling parts are accelerated to velocities that are relatively less when compared to the projectile's velocity. This large-scale but slower-moving recoiling mass can be stopped through the recoil mechanism in 0.2 s to 0.5 s (within a tolerable recoil stroke). Using a recoil force $K(t)$ that decreases the velocity of the recoiling parts, as shown in Figure 2-2, the peak value of the recoil force is lower than the peak value of the internal ballistic force (DOD, 1988).

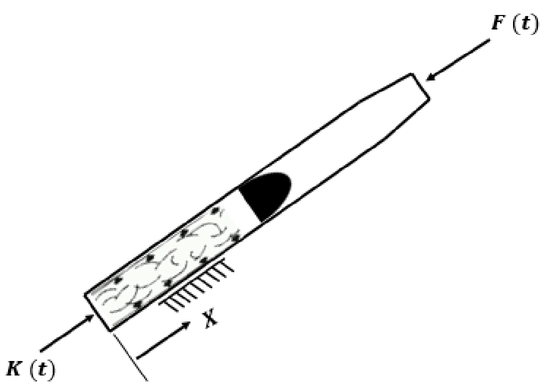

Figure 2-2: Forces acting on recoiling parts

2.5 Components of a Recoil Mechanism

A recoil mechanism is comprised of three basic components:

- a recoil brake to put a rest to the recoiling parts;
- a counter-recoil mechanism that returns the barrel to the position of the barrel before firing (battery position); and
- a buffer that regulates velocity during counter-recoil.

A piston assembly and hydraulic cylinder piston assembly are part of the recoil brake. The movement of the piston in the cylinder creates a force by restricting the hydraulic fluid flow from the chamber of the cylinder. The value of this restricting force depends on the flow of fluid within one or more orifices, the size of which is determined during the design stage to offer the required recoil velocity and pressure curves. Recoil energy absorbed by this restricting force dissipates as heat (DOD, 1988).

The counter-recoil mechanism includes a recuperator and a counter-recoil cylinder assembly, which may be a different unit or may be the recoil brake components that are acting in the opposite direction. At times, the terms counter-recoil mechanism and recuperator are used synonymously. In this study, the recuperator is the equipment that stores some of the recoil energy for counter-recoil, while the counter-recoil mechanism is the unit that returns the recoiling parts back to the battery position. The counter-recoil mechanism obtains its energy from the recuperator.

There are two main types of recuperators, namely a spring mechanism and a hydro-pneumatic mechanism. The spring mechanism stores the energy needed to return the gun to the battery position in a mechanical spring(s). Conversely, the hydro-pneumatic mechanism usually stores this energy in compressed gas. A recuperator force is always present to keep the recoiling parts in-battery at every elevation angle. There is additional compression of the spring or gas during recoil, storing the additional energy required for counter-recoil. The function of the buffer mechanism is identical to the recoil brake but at lower levels of energy. Energy at the end of counter-recoil should be absorbed, as there must be ample recuperator energy to bring the recoiling parts into the battery at a rapid velocity. If this energy is not regulated, then the weapon might tumble over its fixtures (nose over) when returning to the battery due to a sudden stop, or might suffer structural damage, or both (DOD, 1988). While both types of recuperators are introduced, this study focused mainly on the spring mechanism.

2.5.1 Recuperator

Mechanical springs are commonly used as the recuperator for light weapon systems whilst pneumatic cylinders are commonly used in larger systems. The recuperator is commonly located concentrically or parallel to the tube of the gun. The mounting method relies on the size of the recuperator required, its location, the available space and the effects of the eccentric forces because of the variation and alignment errors (DOD, 1988).

Mechanical springs are only used in applications which require very short recoil length, for example, the 40 mm gun system used in this research. In these types of applications, a spring coil can give enough counter-recoil force. If such type of spring is designed with the proper safety guidelines against the breakage, a reliable and simple mechanism is attained (DOD, 1988).

2.6 Vibration Background

This section introduces the vibration subject concisely. The word ‘vibrations’ is often used synonymously with ’oscillations’ to describe motions. Vibration refers to any movement that repeatedly occurs after a given interval of time. Examples of vibrations include the movement by a plucked string and swinging a pendulum. The theory of vibration studies and explains the oscillatory motion of bodies and the associated forces (Bhave, 2010).

2.6.1 Mass-spring vibrating system

The mass element stores and releases kinetic energy, and the spring element stores and releases potential energy. The vibration of a system allows for the transfer of potential energy to kinetic energy. The process can occur alternatively, where the kinetic energy is then transferred back to its potential energy (Piersol & Paez, 2002).

2.6.2 SDOF

Figure 2-3 displays a system consisting of a spring and mass that illustrates the most basic oscillating system. An SDOF system has only one coordinate, i.e. the x-coordinate that can determine the position of mass at any moment. The movement caused by the disturbance at the starting point is to be free of vibration because no extrinsic force is exerted to the mass (Paz & Leigh, 2004). Where the mass is m, with a spring with a stiffness coefficient k.

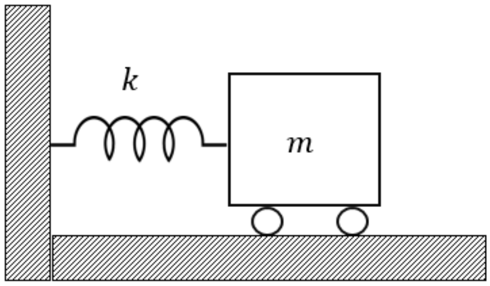

Figure 2-3: Spring and mass system in horizontal position

2.6.3 Vibration classification

The essential vibration classifications used in physics are discussed in this section.

2.6.3.1 Free and forced vibration

Bodies or objects often oscillate upon disturbance. However, in free vibration, the system continues to oscillate on its own when free from interference. At the point of free oscillation, there is no external force acting on the object or body. The swinging of a pendulum is a typical example of free system vibration. Conversely, forced vibration results when an external force acts on the system. The vibration is often a result of a repeated external force (Piersol & Paez, 2002). At times, the natural frequencies of the oscillating bodies and the frequency arising from external force coincide, leading to a condition called resonance (in the absence of damping).

2.6.3.2 Undamped and damped vibration

If no element is present that generates or dissipates energy whilst the movement of the mass, the amplitude of movement with respect to time stays the same; this is an undamped system. When considering real world conditions, the free vibration's amplitude with respect to time lessens slowly, because of the resistance caused by the surrounding medium (for instance, air). These types of oscillations are known to be damped (Rao, 2011).

2.7 Resistive Recoil Force Model (RR):

According to STANAG 4367, Figure 2-4 illustrates how the gun system acts during firing. When the breech force exceeds the preloaded force of the recoiling system, the barrel starts to accelerate backwards at (t_{r0}). With respect to time, the force exerted by the recoil mechanism is increased almost linearly to the projectile ejection. After projectile ejection, the barrel is still accelerating backwards to (t_r) (STANAG-4367, 2000).

For internal ballistics representative weapon specific RR curves integrated into the internal ballistic model is crucial to obtain the effect of recoiling on the projectile muzzle velocity (Schabort, 2016). Literature on RR curves is limited and when available broadly generic since this type of information is intellectual property for gun manufacturers. In addition, RR curves are not the same for all weapon systems.

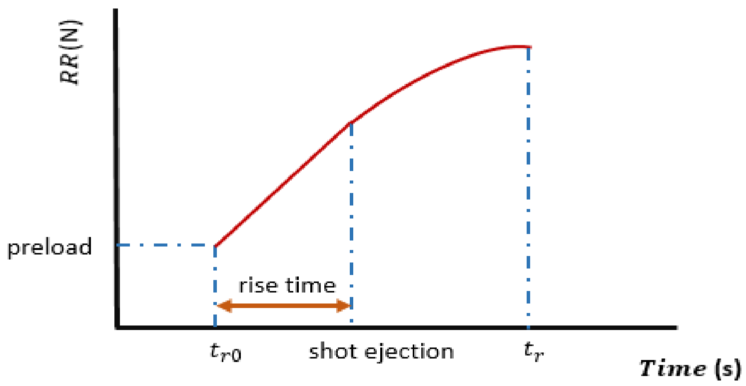

Figure 2-4: Weapon recoil vs time (STANAG-4367, 2000)

2.8 Impulse and Momentum

Newton's 2nd law of motion led to the derivation of the concept of impulse and momentum. In this context, linear impulse and linear momentum must be considered first. During the firing stage it is assumed that there is only an impulsive force due to propellant combustion acting on the barrel. By writing $v = \dot{x}$, Equation 3-1 may be written as follows:

$$F = m\frac{dv}{dt}, \quad (2\text{-}1)$$

where F represents the impulsive force. From Equation 2-1, it follows through separation of variables, that:

$$\int_{t_0}^{t_1} F\,dt = m\int_{v_0}^{v\_1} dv, \quad (2\text{-}2)$$

which may be written as:

$$\int_{t_0}^{t_1} F\,dt = mv_1 - mv_0 = \Delta\,v, \quad (2\text{-}3)$$

where the left-hand side of Equation 2-3 represents the impulse and the right-hand side the change in momentum. Equation 2-3 describes the principle of linear momentum and impulse.

The impulse of a force vs time is a relatively large magnitude that acts over a small interval of time. The impulse can be obtained from the area under the force vs time curve.

When considering a system of more than one body, Equation 2-1 may be written as:

$$\sum F_i = \sum m_i \frac{dv_i}{dt}, \tag{2-4}$$

where $\sum F_i$ represents the impulsive forces due to all external forces, and i indicating the body. By integratin Equation 2-4, it follows that:

$$\int_{t_0}^{t_1} F_i \, dt = \sum m_i (v_i)_1 - \sum m_i (v_i)_0. \tag{2-5}$$

If the sum of all external forces on the system of bodies are zero, the conservation of linear momentum follows from Equation 2-5:

$$\sum m_i (v_i)_1 = \sum m_i (v_i)_0. \tag{2-6}$$

2.8.1 Conservation of momentum for a weapon system

The conservation of momentum for a weapon system can be derived by assuming the following:

- The total momentum before the firing is zero, i.e. $\sum m_i (v_i)_1 = 0$.
- After firing it is assumed that all the propellant burnt out, and that the propellant mass m_c, and the projectile mass m_p, exit the muzzle with the same velocity v_p.

If the positive direction is taken towards the right Figure 3-5, from Equation 2-6 it then follows that:

$$0 = \left(m_p + m_c\right) v_p - m_r v_r, \tag{2-7}$$

where m_r and v_r are respectively the mass and the velocity of the recoiling parts.

From Equation 2-7 it then follows that:

$$m_r v_r = \ m_p v_p + m_c v_c. \tag{2-8}$$

Therefore, the velocity of the recoiling mass can be described by the following equation (Horn & Boutteville, 1982):

$$v_r = \frac{(m_p + m_c)v_p}{m_r}. \quad \text{2-9}$$

2.9 Summary

This chapter provided a review of the literature regarding recoil systems and described the roles that a recoil system plays in a ballistic system. It also explained the various recoil subsystems and components, as well as the forces acting on them during the ballistic cycle. The conservation of momentum for a weapon system and recoil, impulse and momentum were also discussed. The chapter introduced the concepts that are critical to the study. In the following chapter, the recoil modelling will be discussed in detail.

CHAPTER 3 – RECOIL MODELLING

3.1 Introduction

This chapter introduces 40 mm ammunition, the weapon system, the FBD of the weapon system and the weapon system setup. It also derives the governing equations, formulates the numerical model of the gun recoil system and derives the analytical model. As was mentioned in the limitations of this study, the damping of the recoil model is excluded because the weapon system (40mm) comprising of only an equivalent linear spring stiffness recoil element.

3.2 Ammunition and Weapon System

The 40 mm high velocity (HV) ammunition, depicted in Figure 3-1, is known for a muzzle velocity of approximately 240 m/s and a maximum effective range of 2,000 metres (Gander, 2002). It has a typical breech pressure of less than 80 MPa.

Figure 3-1: 40 mm HV ammunitions

The 40 mm HV ammunition is generally fired from an automatic grenade launcher (AGL) mounted on a tripod. The weapon system is considered an area weapon with a typical firing rate of 300 rounds per minute (depending on the limitations of the AGL or ammunition) (Gander, 2002).

A proof weapon is a single-shot, purpose-built weapon designed to measure specific parameters related to the ammunition such as pressure and acceleration from when the firing pin strikes the primer percussion cap until the projectile exits the muzzle of the weapon, also known as the action time. Proof weapons are normally used when testing for specific conditions related to ammunition. This type of weapon is consequently used for this research, as introduced in Chapter 1. Although this type of weapon is not an exact representation of a typical AGL, it provides a purpose-built replica. The recoil mass, breech configuration and barrel dynamics will be different. However, the process steps followed in this study remains the same for any weapon system.

The 40 mm HV proof weapon comprises of a test barrel known as the Electronic Pressure, Velocity and Action Time (EPVAT) barrel mounted with support and safety devices / bolt assembly as shown in Figure 3-2, according to the requirements of STANAG AC/225(LG/3-SG/1)D/17.

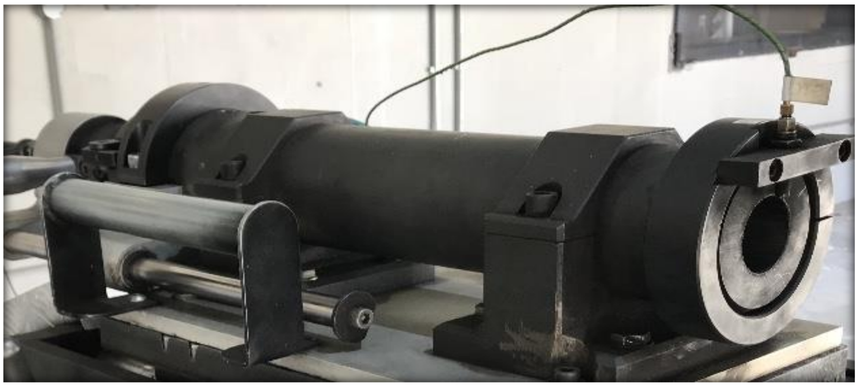

Figure 3-2: 40 mm HV proof weapon

The following section details the method of setting up the proof weapon.

3.3 40 mm HV Proof Weapon Setup

The proof weapon is mounted on a recoil platform fixed to a concrete support structure as depicted in Figure 3-3. When the breech of the weapon is closed, the firing pin, breech and barrel form a closed chamber in which the ammunition propulsion system combusts. The recoil platform provides recoil movement to the weapon mass (when fired) by means of linear bearings and spring stiffness elements mounting the recoil plate to the concrete support structure.

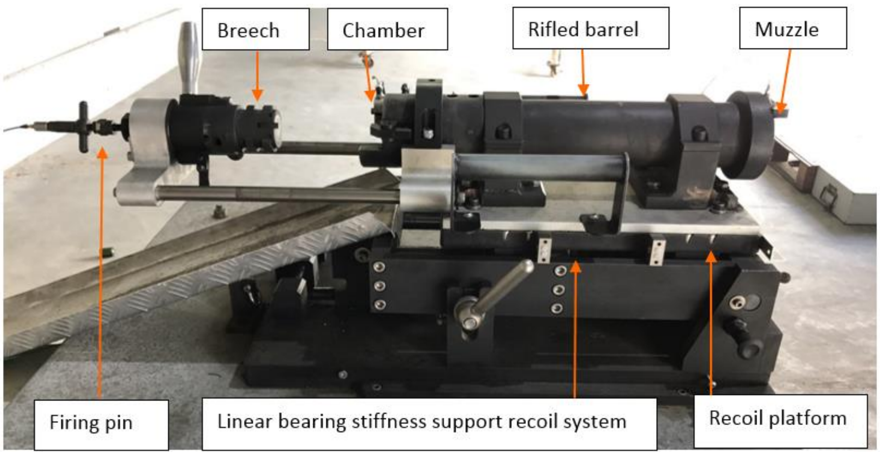

Figure 3-3: 40 mm HV proof weapon / test setup

3.4 FBD – Weapon Setup

In this study, the recoil motion of the weapon system is approximated as an SDOF mass-spring system. Figure 3-4 shows a typical representation of the weapon system, where the mass of the barrel is m, with a spring with a stiffness coefficient k. This representation forms the basis of the considered recoil model.

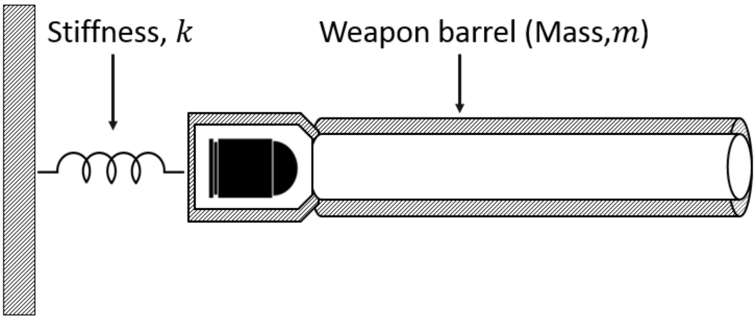

Figure 3-4: SDOF representation of weapon system

The FBD of the weapon platform and weapon / barrel is shown in Figure 3-5. As discussed elsewhere in this document, kx represents the spring force as a result of a compression x, $\ddot{x}$ is the acceleration, and $F(t)$ the driving or exciting force.

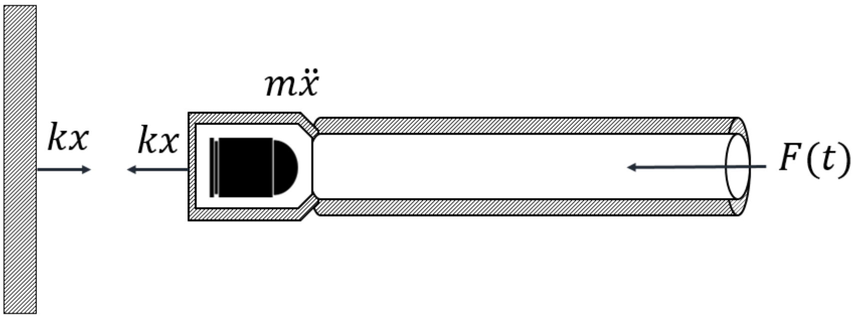

Figure 3-5: Weapon platform and weapon FBD

3.5 Governing Differential Equations

The governing equations will be derived using Newton's 2nd law of motion and the procedure identified below:

- Use a suitable coordinate of the weapon system to describe the location of the weapon mass contained within the system.
- Determine the static equilibrium configuration of the weapon system.
- Draw the FBD of the weapon mass when it is exposed to positive displacement.
- Indicate all active and reactive forces acting on weapon mass.

- Apply Newton's 2nd law of motion to the weapon’s mass shown by FBD.

From Newton’s second law of motion it follows that:

$$\sum F = m\frac{d^2x(t)}{dt^2} = m\ddot{x}, \tag{3-1}$$

where $\ddot{x}$ is the acceleration, and $\sum F$ represents all the external forces acting in on of mass m.

When the body is displaced by a distance of $+x$ in a horizontal direction, the force stored in the spring is kx. If an additional exciting force $F(t)$ is acting on the body, then from Equation 3-1 it follows that:

$$-kx + F(t) = m\ddot{x}. \tag{3-2}$$

Equation 3-2 can then be re-arranged, yielding:

$$F(t) = m\ddot{x} + kx. \tag{3-3}$$

The different terms in Equation 3-3 represent the following:

$F(t)$ - *Excitation force (gas pressure force)* (N)

The input (excitation) force is the impulse generated by the propellant gas pressure. This force acts on the gun breech until the projectile and propellant gas have exited the weapon barrel.

$(m\ddot{x})$ – *Represents the response of the mass due to the external forces* (N)

The entire mass of the weapon system is considered as the recoiling mass, implying that all mass is moving with the weapon during a firing cycle.

(kx) - *Spring force on recoiling mass* (N)

When compressed or extended beyond its equilibrium length, a linear spring element will exert a force proportional to the deflection on any system attached to the spring element. A mass that compresses a spring element will always experience a counterforce that strives to restore the system to its rest or equilibrium position. Upon compression / extension, the spring force increases potential energy and returns that energy into the recoiling mass. As illustrated in Figure 3-6 below, the absence of damping in a recoil system will result in a continually oscillating system.

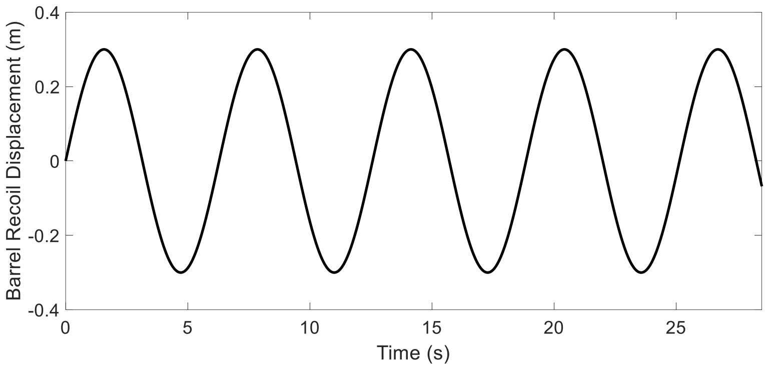

Figure 3-6: Barrel recoil vs time

The spring force associated with the weapon system refers to the counterforce that acts on the recoil frame while the mass recoils.

As introduced in Section 1.5, the weapon system considered for this study does not include damping.

3.6 Numerical Model Formulation (Runge-Kutta method)

A numerical simulation model based on an SDOF spring was derived using the Runge-Kutta fourth-order method. The second-order differential equation shown in Equation 3-3 is written as two first-order differential equations.

For this, a representation of unknown functions is introduced as:

$$\frac{dx}{dt} = h(x, v, t), \tag{3-4}$$

$$\frac{dv}{dt} = g(x, v, t). \tag{3-5}$$

Equation 3-3 can be rewritten as:

$$g(x, v, t) = F(t) - kx(t). \tag{3-6}$$

Equation 3-6, along with the second relation given in Equation 3-4 and 3-5, can be expressed as:

$$h(x, v, t) = v(t). \tag{3-7}$$

The numerical solution for the two differential equations is as follows:

$$x_{i+1} = x_i + \frac{1}{6}[k_o + 2k_1 + 2k_2 + k_3], \tag{3-8}$$

$$v_{i+1} = v_i + \frac{1}{6}[l_o + 2l_1 + 2l_2 + l_3]. \quad 3\text{-}9$$

The initial conditions are:

$$x_0 = x(t = 0), \quad 3\text{-}10$$

$$v_0 = v(t = 0). \quad 3\text{-}11$$

And:

$$k_0 = hf(x_i, v_i, t_i), \quad 3\text{-}12$$

$$l_0 = hg(x_i, v_i, t_i), \quad 3\text{-}13$$

$$k_1 = hf\left(x_i + \frac{1}{2}k_0, v_i + \frac{1}{2}l_0, t_i + \frac{1}{2}h\right), \quad 3\text{-}14$$

$$l_1 = hg\left(x_i + \frac{1}{2}k_0, v_i + \frac{1}{2}l_0, t_i + \frac{1}{2}h\right), \quad 3\text{-}15$$

$$k_2 = hf\left(x_i + \frac{1}{2}k_1, v_i + \frac{1}{2}l_1, t_i + \frac{1}{2}h\right), \quad 3\text{-}16$$

$$l_2 = hg\left(x_i + \frac{1}{2}k_1, v_i + \frac{1}{2}l_1, t_i + \frac{1}{2}h\right), \quad 3\text{-}17$$

$$k_3 = hf(x_i + k_2, v_i + l_2, t_i + h), \quad 3\text{-}18$$

$$l_3 = hg(x_i + k_2, v_i + l_2, t_i + h). \quad 3\text{-}19$$

3.7 Analytical Model (response to harmonic excitation)

Harmonic excitation for undamped systems refers to a sine or cosine external force of a frequency applied to a system. Resonance is the response of a system to harmonic excitation. Resonance occurs when the external excitation has the same frequency as the natural frequency of the system. The harmonic excitation module utilises the equations for the response of an SDOF system with no damping to harmonic excitation using a mass-spring model.

Consider a simple mass-spring system with a frictionless surface subjected to a harmonic excitation force, for simplicity. If an excitation force $F(t) = F_0\cos(\omega t)$ acts on the mass m of mass-spring system, the equation of motion, Equation 3-3, yields

$$m\ddot{x} + kx = F_0 \cos(\omega t). \quad \text{3-20}$$

In the given equation, F_0 represents the amplitude of the driving force while ω is the angular frequency of the force exerted.

The homogeneous solution of this equation is given by:

$$x_h(t) = A\cos\omega_n t \ + \ B\sin\omega_n t. \quad \text{3-21}$$

In Equation 3-21, $\omega_{n=}\sqrt{\frac{k}{m}}$ represents the system's natural frequency. Because the exciting force $F(t)$ is harmonic, the particular solution $x_p(t)$ also takes the form of a harmonic response and has the same frequency ω. Thus, the following form of the solution is assumed:

$$x_p(t) = X\cos(\omega t), \quad \text{3-22}$$

where X denotes the maximum amplitude of $x_p(t)$

Substituting Equation 3-22 into Equation 3-20 and solving for X yields the solution

$$X = \frac{F_0}{k \ - \ m\omega^2}. \quad \text{3-23}$$

Hence, the analytical solution of Equation 3-20 yields:

$$x(t) = A\cos(\omega_n t) + B\sin(\omega_n t) + \frac{F_0}{k - m\omega^2}\cos(\omega t). \quad \text{3-24}$$

The initial conditions to solve the above equation are:

$$x(t = 0) = x_0, \quad \text{3-25}$$

$$\dot{x}(t = 0) = \dot{x}_0. \quad \text{3-26}$$

The following are found:

$$A = x_0 - \frac{F_0}{k - m\omega^2}, \quad B = \frac{\dot{x}_0}{\omega_n}. \quad \text{3-27}$$

Thus, the governing differential equation for the analytical model can be defined as:

$$x(t) = \left(x_0 - \frac{F_0}{k - m\omega^2}\right)\cos(\omega_n t) + \left(\frac{\dot{x}_0}{\omega_n}\right)\sin(\omega_n t) + \left(\frac{F_0}{k - m\omega^2}\right)\cos(\omega t). \qquad 3\text{-}28$$

3.8 Summary

This chapter introduced 40 mm ammunition, the weapon system, the FBD of the weapon system and the weapon system setup. The governing differential equations were derived using Newton's second law method of motion in this chapter. In addition, this chapter formulated the numerical model of the gun recoil system (the fourth-order Runge-Kutta method). Finally, the chapter derived the analytical model (the harmonic excitation). In the following chapter, the numerical model will be implemented and verified against analytical model.

CHAPTER 4 - SIMULATION MODEL

4.1 Introduction

In this chapter, the fourth-order Runge-Kutta numerical model will be programmed using MATLAB. The numerical simulation program serves the main aim of this research, which is to predict the spring stiffness of a weapon system using an iterative process. Finally, the numerical simulation model will be verified against the analytical model to establish the correct execution of the iterative model. The purpose of the verification is to ensure the accuracy of the numerical simulation model, which will then be used with confidence with data gathered from experimental measurements in Chapter 6.

4.2 Numerical Method

In this section, the focus is on the numerical model that is used to solve an SDOF system that is subjected to an external forcing function. The behaviour of systems regarding changes to its parameters can be best understood using analytical solutions. Analytical solutions based on suitable parameter values can help obtain specific response characteristics when designing a system. An appropriate numerical integration procedure can be used to find the response of the systems, especially in the cases where analytical solutions are difficult to obtain. Various methods are available for numerically integrating ordinary differential equations.

Analytical models with exact solutions are tedious and often complex to use, especially when finding the response of a system when the excitation or forcing function cannot be described in simple analytical forms. It is particularly hard to use when the force data are experimentally determined and used in the analysis (Rao, 2011). For this reason, numerical models are used to determine the response of systems subjected to forcing functions.

Multiple numerical methods are available, with only slight differences among them. Methods such as Runge-Kutta are popular for the numerical solution of differential equations (Hoffman, 1992). The implementation of these numerical methods can be challenging, and results need to be ‘checked’ for the correct use before results can be trusted. For this study, the process of checking the method for correctness is referred to as verification and is further discussed in Section 4.5. ‘Simplified dummy models’ (made up case studies) which can be analytically described with an exact solution can be used to verify a numerical model.

A numerical simulation model based on an SDOF spring was derived in Section 3.6 using the fourth-order Runge-Kutta method in the computer software package MATLAB. The model can identify the equivalent system spring stiffness.

The fourth-order Runga-Kutta integration method was chosen because it is accurate and reasonably efficient (fast). Based on a single-step method, it allows for dynamically adjusting the integration step if needed. Outputs can easily be gained at any time step, which is helpful while debugging.

4.3 Time Step

The accuracy of the simulated spring stiffness coefficient is dependent on the model integration time step. The time step can be changed depending on the weapon system type and its expected dynamic response.

4.4 Simulation Model Algorithms

A fourth-order Runge-Kutta integration is used to predict the spring stiffness of the weapon system numerically. The equivalent spring stiffness is iterated until convergence between simulated and measured displacement is achieved using the data gathered from experimental measurements as inputs to the model.

This process includes sequential steps as shown below:

1. Read all the measured inputs (total recoiling mass value, breech force data and displacement data);

2. Iterate the numerical model solution for various spring stiffness coefficients while comparing the simulated displacement to the actual measured data;

3. Use the solution that yields the smallest comparative error as a centre coefficient to re-iterate various spring stiffness coefficients; and

4. Repeat the above process until the solution converges.

The numerical model code is provided in detail within Appendix A.

4.5 Model Verification

The main objective of the verification process is to determine the correctness of the computational and programming implementation of the model. Verification examines the mathematical aspects within the model through a comparison of the modelled results with exact analytical results. The verification process can further be utilised to check for programming errors (AIAA, 1998). However, program verification is conducted to determine whether the program is accurately implemented. An analytical model case study with known mass and spring stiffness, as presented in Section 3.7, will be used to generate an excitation force and positional data. The generated data will then be used as inputs to the numerical model to verify whether the numerical model converges to the corresponding spring stiffness utilised to generate the data. The verification process is illustrated in Figure 4-1.

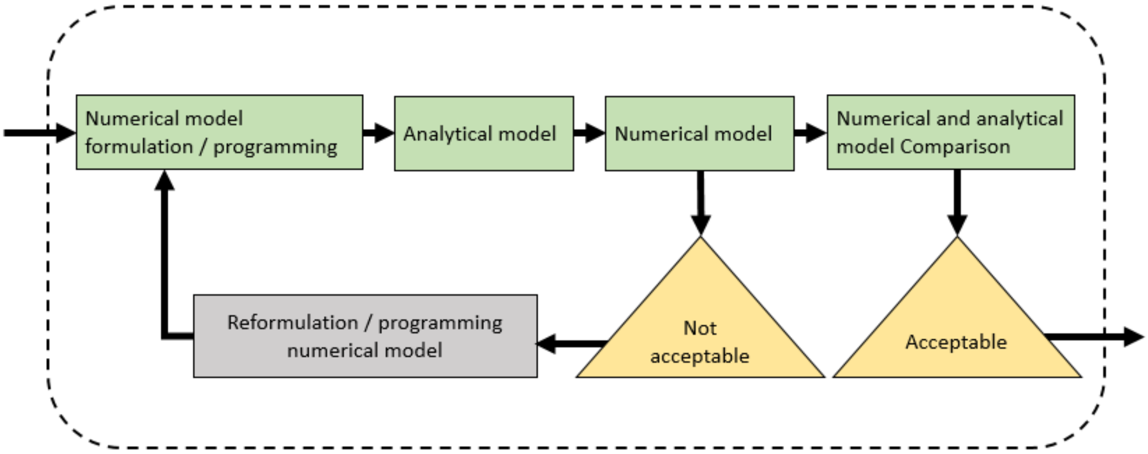

Figure 4-1: Verification process flowchart

1. Numerical model formulation / programming: The numerical model is formulated and programmed (Section 4.4).

2. Analytical model: An analytical model based on an undamped SDOF system that is exposed to a harmonic excitation (a type of force that is not intended to represent the input / impact force of this study but rather to make the solution easily determinable) is used to generate displacement and excitation force data. This type of model is used because the solution to this model is exact and can be used for comparison purposes.

3. Numerical model: A numerical model formulated and programmed as part of this study utilise the data (displacement and excitation force) generated by the analytical model as inputs. The numerical model is then used to predict the SDOF system spring stiffness that was used by the analytical model to generate the data.

4. Numerical and analytical model comparison: The output datasets are compared and the converged system stiffness is numerically evaluated against the spring stiffness of the analytical model.

4.5.1 Generating analytical data

The analytical model, which is based on an undamped SDOF system, is used to generate data when an excitation force function acts on the mass. Figure 4-2 (a) shows the excitation force vs time. The initial conditions consist of an excitation force (90000 N) at omega (10 rad/s), a spring stiffness (19000 N/m) and a mass value (90 kg). Figure 4-2 (b) shows the displacement over time; the initial condition for displacement is 9 m.

The analytical model was discussed in Chapter 3. The analytical model code is presented in detail in Appendix A.

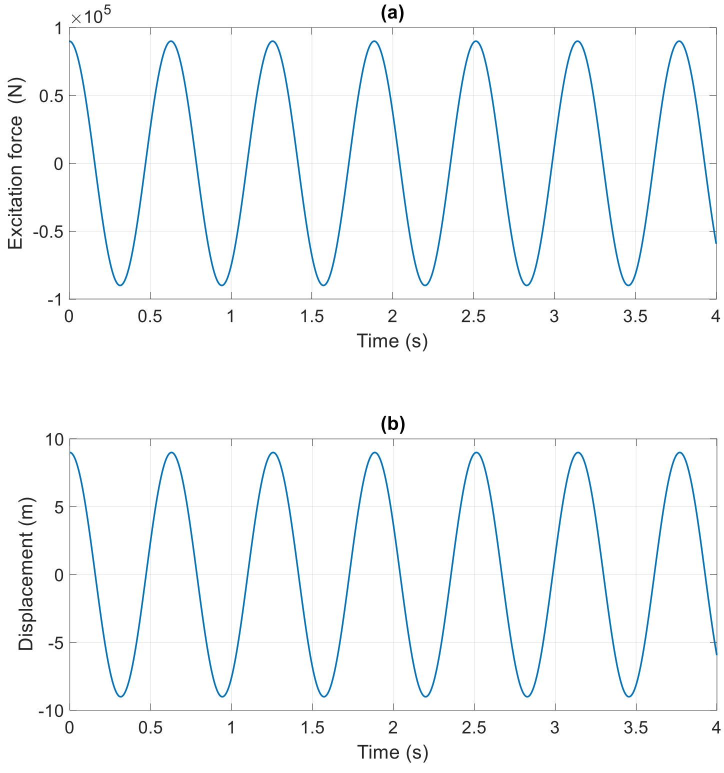

Figure 4-2: Data generated – (a) Excitation force vs time, (b) Displacement vs time

4.5.2 Comparing analytical and numerical models

The generated excitation force, displacement analytical data and mass were given to the numerical simulation model as inputs to identify the spring stiffness value by means of an iterative process as shown in Figure 4-3.

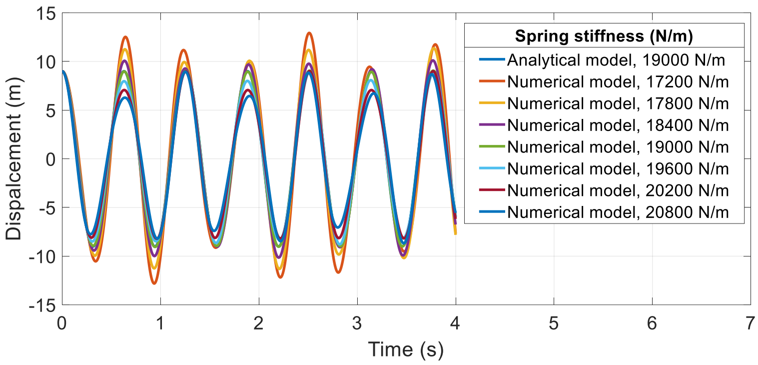

Figure 4-3: Displacement vs time (numerical model and analytical model comparison)

As can be seen from Figure 4-3, the spring stiffness value of the numerical model solution that yields the smallest comparative error is 19000 N/m. Figure 4-4 presents the numerical model displacement that yields the smallest comparative error to the analytical model displacement. The spring stiffness (19000 N/m) used in the analytical model (used to generate the data) was compared to the spring stiffness identified by the numerical model (shown in Table 4-1). Therefore, the two stiffness values are correlated. Consequently, the model is considered to be verified.

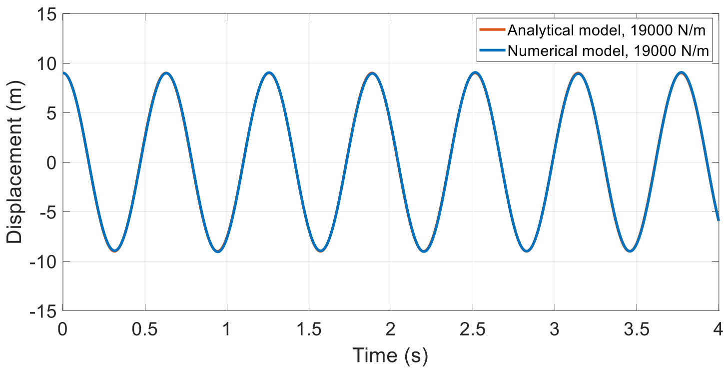

Figure 4-4: Displacement vs time and (numerical model and analytical model comparison)

Table 4-1 shows the predicated spring stiffness value of the numerical model program and the analytical model spring stiffness value.

Table 4-1: Numerical model vs analytical model equivalent spring stiffness

Predicated spring stiffness of the numerical model (N/m)	19000
Spring stiffness from analytical model (N/m)	19000

Table 4-1 demonstrates that the predicted spring stiffness of the numerical model program correlates to the spring stiffness used in the analytical model. At this point, the numerical simulation program will be used with confidence with data gathered from the experimental measurements presented in Chapter 5.

4.6 Summary

This chapter focused on the numerical model formulated using a computer program. The numerical simulation model was verified using an analytical model of a simplified undamped SDOF system. The verification process proves the accuracy of the numerical simulation model and can consequently be used with confidence with data gathered from the experimental measurements to be discussed in Chapter 6.

Chapter 5 will introduce the characterisation of 40 mm HV proof weapon elements, as well as the experimental methodology.

CHAPTER 5 - EXPERIMENTAL SETUP AND CHARACTERISATION

5.1 Introduction

This chapter focuses on two primary aspects. This chapter will firstly focus on identifying the equivalent spring stiffness of the weapon system and the equivalent mass. The equivalent spring stiffness will be identified by means of a load-deflection test for the spring. The equivalent mass will be identified using a digital scale. This chapter will then focus on firing tests, the test setup, the methodology followed to obtain the measured data and the processing of the data.

5.2 Weapon System Element Characterisation

Two weapon system elements are available for characterisation, namely mass and spring stiffness. The equivalent mass is used as an input to the numerical model program. The equivalent spring stiffness is used for validation of the numerical simulation model in Chapter 6.

The characterisation elements of the weapon system are described in the following sections.

5.2.1 Equivalent mass

The recoiling mass was identified using digital scales (refer to Appendix B). The recoiling plate could not be weighed because it is fixed to the recoil platform. Because the weapon was used daily for production testing purposes, it was not possible to disassemble the recoil plate from the recoil platform. All the dimensions of the recoiling plate were measured using a digital calliper and a measuring tape. The measured dimensions, together with a uniform material density (taken as 7800 kg/m^3 for steel) were used to identify the equivalent mass of the components that could not be physically weighed. The following formula was used for calculating mass:

$$mass = \rho V_{total}\ , \qquad \text{5-1}$$

where ρ represents the uniform material density, and V_{total} represents the total volume of material contributing to mass. The equivalent recoil mass for the weapon system was 91.77 kg.

5.2.2 Equivalent spring stiffness

The characterisation of the equivalent spring system was done by setting up the proof weapon in a static position and applying force in a backward direction onto the platform while recording the deflection of the spring and the applied load. The deflection in the spring was recorded using a linear voltage differential transformer and the applied load was measured by means of a load cell. (Refer to Appendix B for more details.)

Using the spring stiffness equation $k = \frac{f}{x}$, where k represents the equivalent spring stiffness, f the applied force, and x the spring deflection, the spring stiffness could be identified as presented in Figure 5-1.

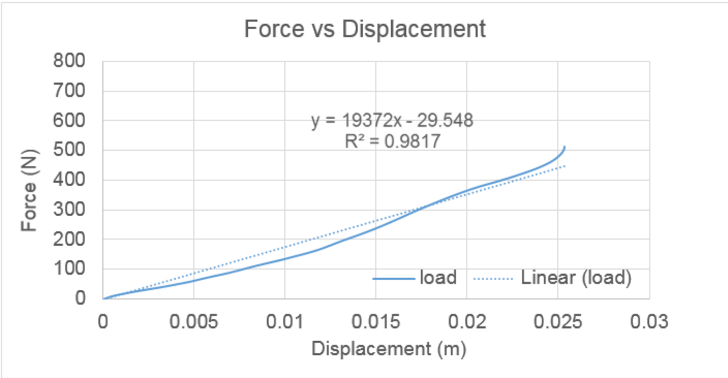

Figure 5-1: Force vs displacement (recoil system)

As can be seen from Figure 5-1 that the equivalent recoil spring stiffness was calculated as 19372 N/m. With a correlation coefficient (R^2) of 0.9817, the confidence in the identified spring stiffness is considered high.

The stiffness magnitude can be also measured by a method named Bump Test. The Bump Test is a test method used to identify resonance frequencies of a vibrating system. If this method was used, it will generate the same stiffness magnitude as obtained from a static load with corresponding deflection test. The purpose of identifying the equivalent stiffness is to validate the simulation result in terms of equivalent stiffness at a later stage. Therefore, the use of the Bump Test method is not essential in this study, because the magnitude of stiffness obtained from the deflection test is adequate.

5.3 Firing Trials

Nine projectiles were fired from the 40 mm HV proof weapon mounted on the recoil platform. The tests were conducted at a proofing test range at Rheinmetall Denel Munition (Pty) Ltd in Somerset West, South Africa.

5.3.1 Test setup & Methodology

Figure 5-2 illustrates the test setup of a 40 mm HV proof weapon mounted on the recoil platform. A piezoresistive accelerometer was used to measure the recoil acceleration of the recoil platform. A high-speed video camera, capable of maintaining a sampling rate of 10000 frames per second (fps), was spaced perpendicular to the weapon’s firing line with the proof weapon in the field of view. This camera was used to track the recoil movement of the proof weapon. A projectile light gate was spaced 4 meters from the muzzle of the proof weapon to measure the muzzle velocity of the projectile. A piezoelectric pressure transducer was used to measure the breech pressure during the firing cycle. A bridge amplifier was used for the signal conditioning of the piezoresistive accelerometer. A charge amplifier was used to convert the charge generated by the piezoelectric pressure transducer to a proportional low impedance voltage output. An analogue-to-digital converter, commonly referred to as a PC-oscilloscope, was used to sample and capture the data readings. (Refer to Appendix B for more details).

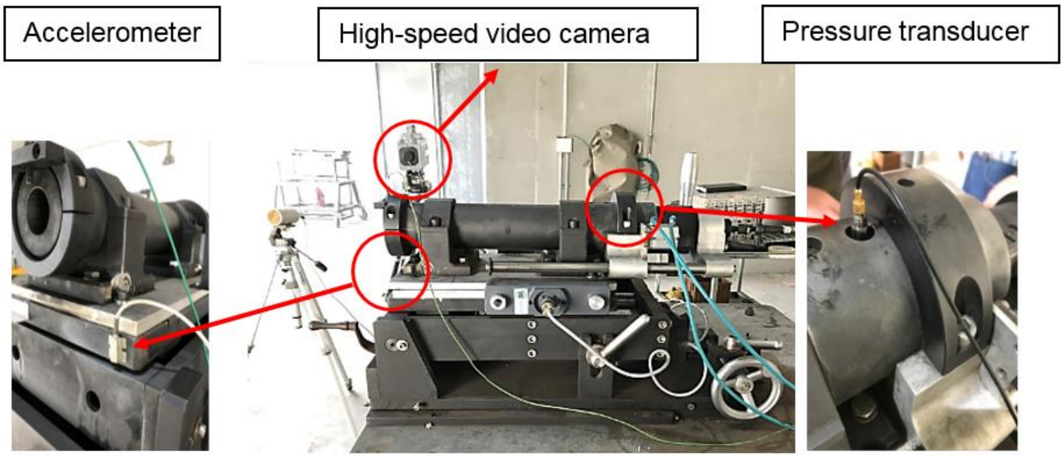

Figure 5-2: Weapon test setup

The flowchart in Figure 5-3 shows the setup of the experimental test discussed above.

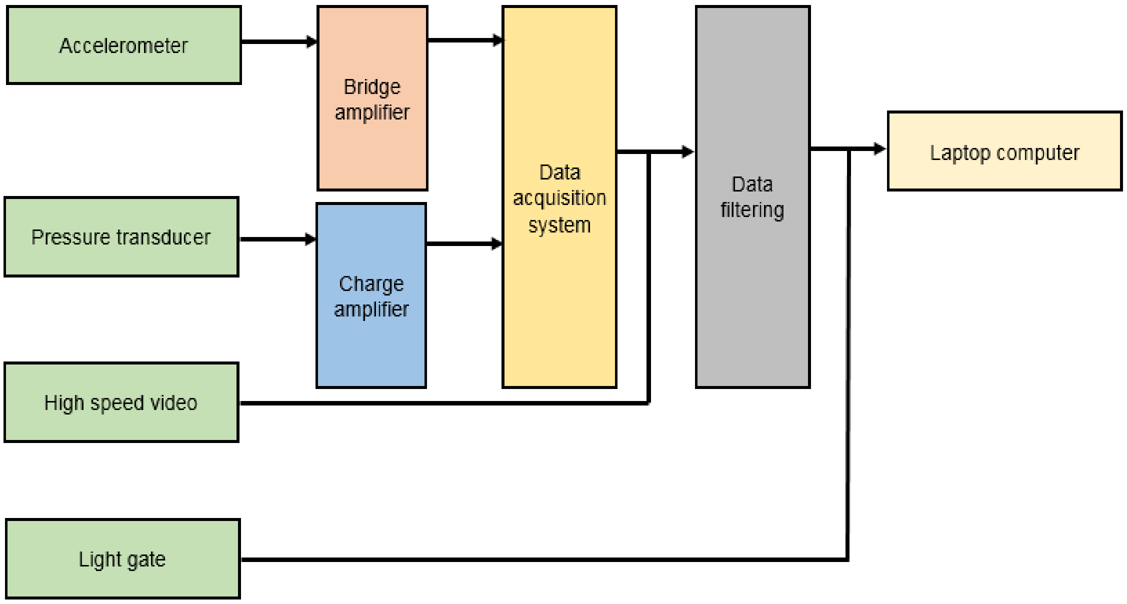

Figure 5-3: Test setup flowchart

The following data were recorded for each of the firings:

- Recoil acceleration measured by the piezoresistive accelerometer with a sample rate and time duration of 5 x 10^{-7} kHz and 1 s.
- Breech pressure measured by the piezoelectric pressure transducer with a sample rate and time duration of 5 x 10^{-7} kHz and 1 s.
- Recoil displacement measured by the high-speed video (HSV) camera with a sample rate and time duration of 1 x 10^{-5} kHz and 0.35 s.
- Muzzle velocity of the projectile measured by the light gate device in front of the proof weapon barrel.
- Time synchronisation: the piezoresistive accelerometer was used to trigger the data-capturing of the various sensors. When an audio sensor triggered the HSV, the audio sensor was also included with the other sensors on the PC-oscilloscope to obtain a timestamp of when the HSV was triggered relative to the other sensors.

5.4 Data Post Processing

The following methodology was applied during data post processing:

Step 1: The breech force was identified by taking the breech pressure measurement, applying a moving average filter of 10 samples and multiplying the measurement with the breech area of the proof weapon. The measurement was filtered to reduce noise due to the excitation of natural oscillations in the pressure measurements resulting from the high rising amplitude of the pressure signal.

Step 2: The recoil displacement was identified using video tracking software (Tracker) and a fixed pixel template (with known dimensions to calibrate the pixels) and tracking the movement of the template for each time / video frame.

The use of the accelerometer to identify the recoil acceleration and velocity (time integral) proved to be inaccurate due to unacceptable large integration errors resulting from high-frequency oscillations in the accelerometer data.

Step 3: The muzzle velocity of the projectile was used to identify the theoretical maximum recoil velocity of the proof weapon (or rather recoiling mass) upon muzzle exit of the projectile by applying a momentum balance between the projectile and recoiling mass.

The muzzle velocity of the projectile was also used to identify the impulse of impact force by making use of the change in momentum of the projectile mass.

An attempt to measure dynamic reaction recoil force was made to obtain additional input for the model to speed convergence using load cells. Unfortunately, it was not possible due to the extent of platform changes needed. it also was not possible at RDM as a production proofing weapon was used to conduct the trial.

5.5 Summary

Throughout this chapter, the identification of the equivalent spring stiffness of the weapon system and mass was performed using a load-deflection test for the spring stiffness and a digital scale for the mass. Also, the chapter discussed several aspects of the test setup, specifically test methodology, firing trail and data post processing. In the following chapter, the experimental results will be provided and discussed. Then, the recoil simulation program will be validated using the data gathered from the experimental measurements.

CHAPTER 6 - EXPERIMENTAL RESULTS AND EVALUATION

6.1 Introduction

In this chapter, the experimental results gathered during firing trials are discussed. The measured acceleration, displacement, breech pressure and muzzle velocity of a 40 mm proof weapon system are presented. Analysis of the data obtained from the firing trials is discussed in detail. The chapter concludes with a comparison between the stiffness identified by the simulation model and the stiffness that was experimentally characterised in the previous chapter.

6.2 Breech Force

The piezoelectric pressure transducer was used to measure the breech pressure. The breech force on the recoiling mass was calculated using the equation, *breech force = breech pressure multiplied by area of the tube gun*. Peak pressure and maximum breech force of approximately 69.1 MPa and 9.108 x 10^4 N, respectively, were identified for shot 6 as an example (all other shots were conducted in a similar manner). The results of breech pressure and the breech force of shot 6 are shown in Figure 6-1.

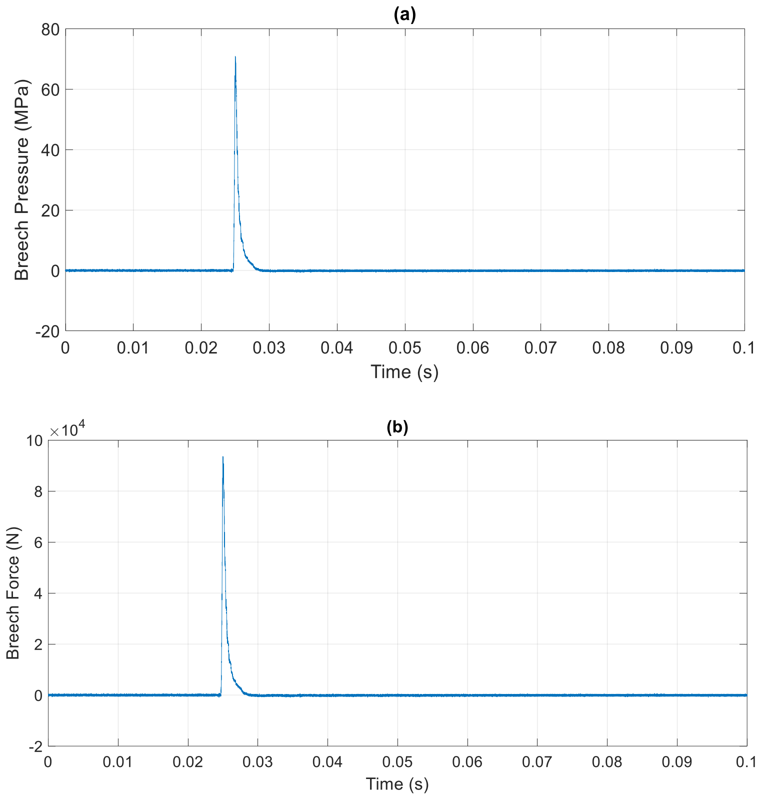

Figure 6-1: (a) Breech pressure vs time and (b) Breech force vs time (shot 6)

Figure 6-2 shows the measurement results of breech pressure and the breech force with a horizontal offset between the curves into the time for nine shots. Table 6-1 below shows the maximum breech pressure and maximum breech force for each shot.

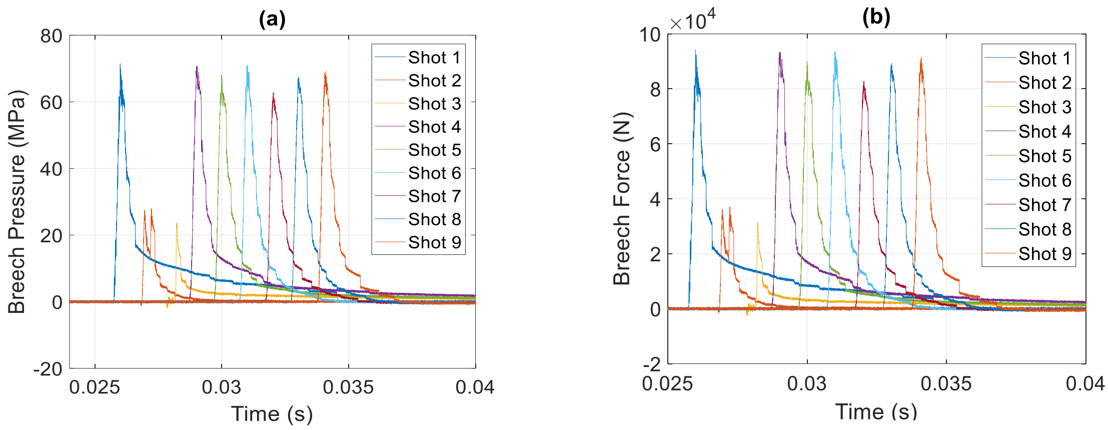

Figure 6-2: (a) Measured breech pressure vs time, (b) Calculated breech force vs time

Table 6-1: Maximum breech pressure and breech force

Shot number	1	2	3	4	5	6	7	8	9
Maximum breech pressure (MPa)	71.4	28.0	23.7	70.6	68.0	70.8	62.7	67.6	69.1
Maximum breech force (N)	94266	11767	31290	93209	28577	93474	822779	89249	91229

6.3 Recoil Displacement and Velocity

Two measurement sources were available for identifying recoil displacement and velocity: HSV and an accelerometer. The displacement identified by each of these sources is explained individually and then compared in the following sections.

6.3.1 High-speed video (HSV)

The Tracker video analysis tool is a software package that enables the identification of multiple variables by analysing a video or an image. The software is designed to be used in physical experiments to measure the displacement and velocity of a moving body (Brown, 2005). The Tracker interface is depicted in Figure 6-3. The video-image pixels are calibrated by a known input assigned between two pixels.

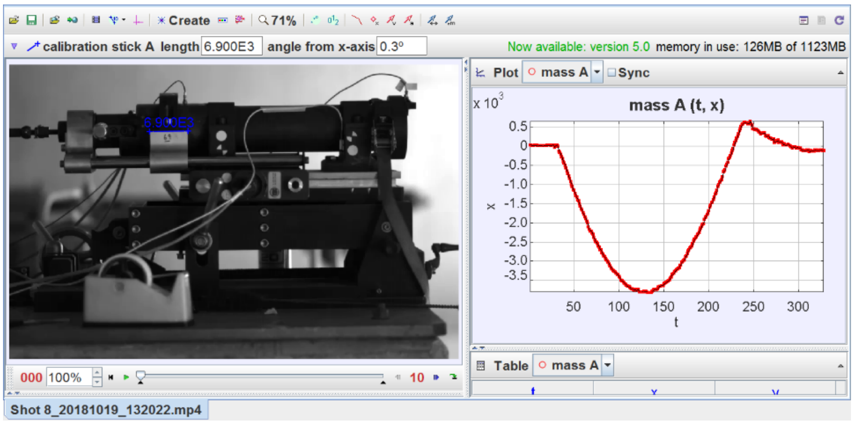

Figure 6-3: Tracker interface

The measured displacement and recoil velocity for shot 6 are shown in Figure 6-4. A maximum recoil displacement and recoil velocity of approximately 0.041 m and 0.66 m/s, respectively, were identified.

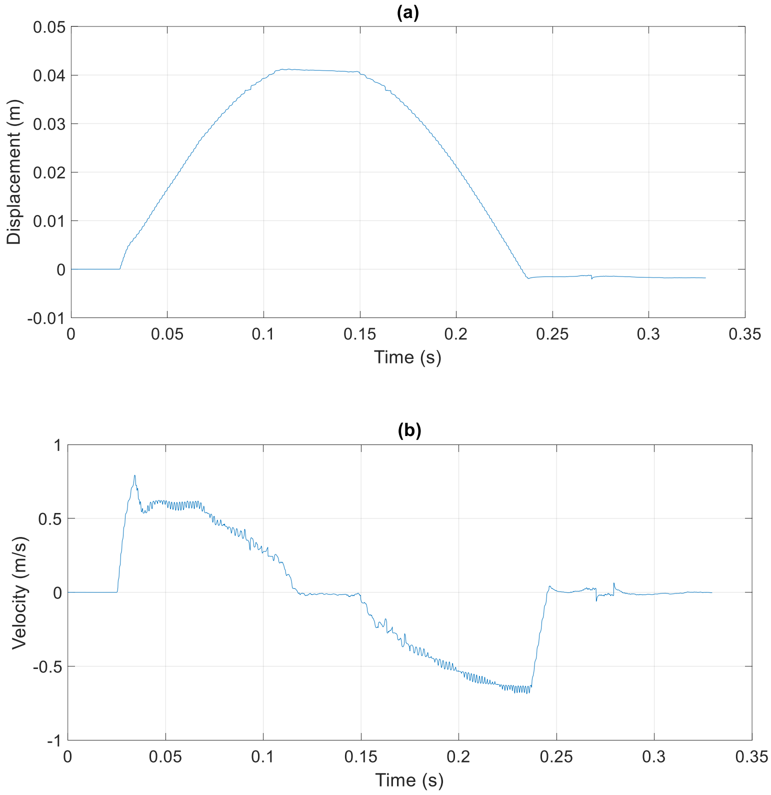

Figure 6-4: (a) Displacement vs time and (b) Velocity vs time (shot 6 using HSV)

Figure 6-5 shows the measurement results of displacement and velocity with a horizontal offset between the curves into the time for nine shots. Table 6-2 lists the maximum displacement and maximum velocity for each shot.

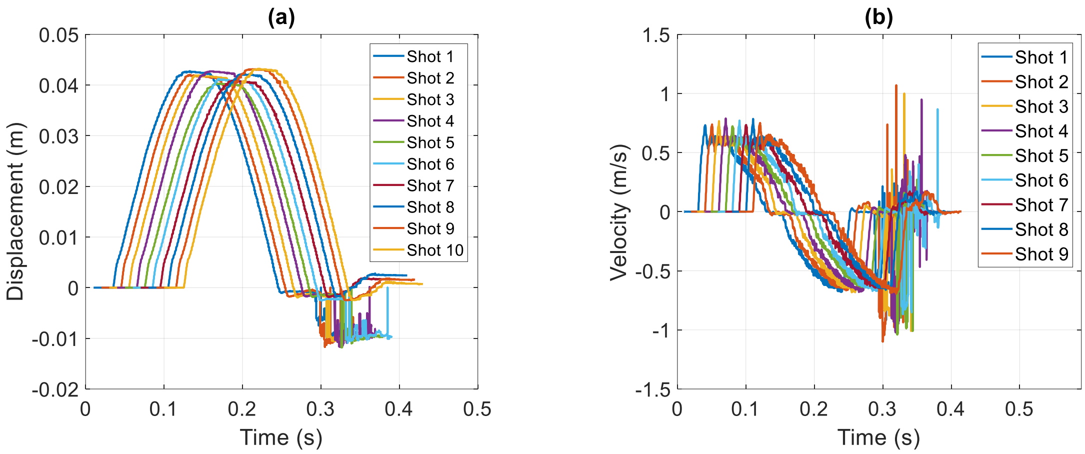

Figure 6-5: (a) Measured displacements vs time, (b) Measured velocities vs time

Table 6-2: Maximum displacement and velocity

Shot number	1	2	3	4	5	6	7	8	9
Maximum displacement (m)	0.043	0.042	0.042	0.043	0.040	0.041	0.041	0.042	0.043
Maximum velocity (m/s)	0.620	0.609	0.608	0.622	0.600	0.605	0.601	0.618	0.629

The displacement vs time curves in Figure 6-5 (a) above indicate only half a cycle. The reason for only half a cycle is that the recoil platform recoils backward (and loads the spring) and then the spring pushes recoil platform back to the original position. When the weapon moves to the front, it hits a metal and rubber stop. In the absence of the metal stop, the weapon would have displaced negatively. Figure 6-6 (a) and (b) illustrates the displacement response for a normal undampened SDOF and a weapon approximated as an SDOF with multiple shots.

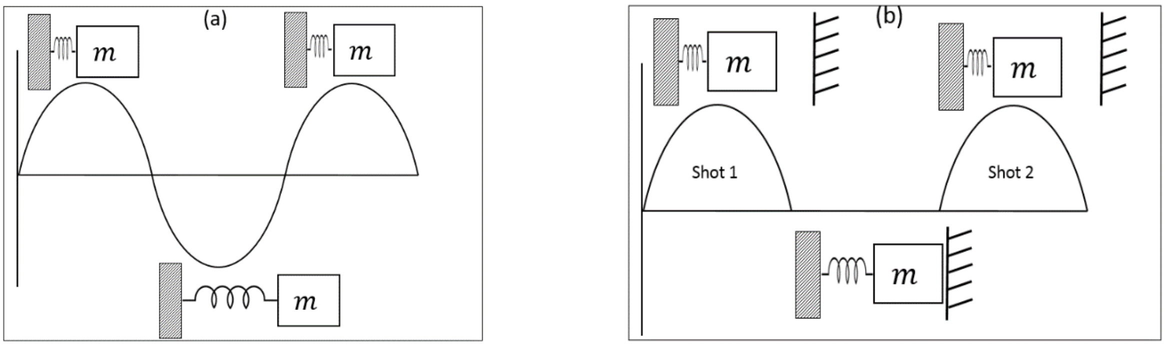

Figure 6-6: (a) Normal undampened SDOF response (b) Approximated as SDOF response

6.3.2 Accelerometer

An accelerometer placed on recoil mass was also used to measure recoil acceleration for each round fired to integrate the signal for recoil velocity. The recoil velocity could be identified by integrating the measured acceleration. The recoil acceleration measured for shot 6 (as an example), as well as the recoil velocity calculated as the first integral of recoil acceleration, are shown in Figure 6-7.

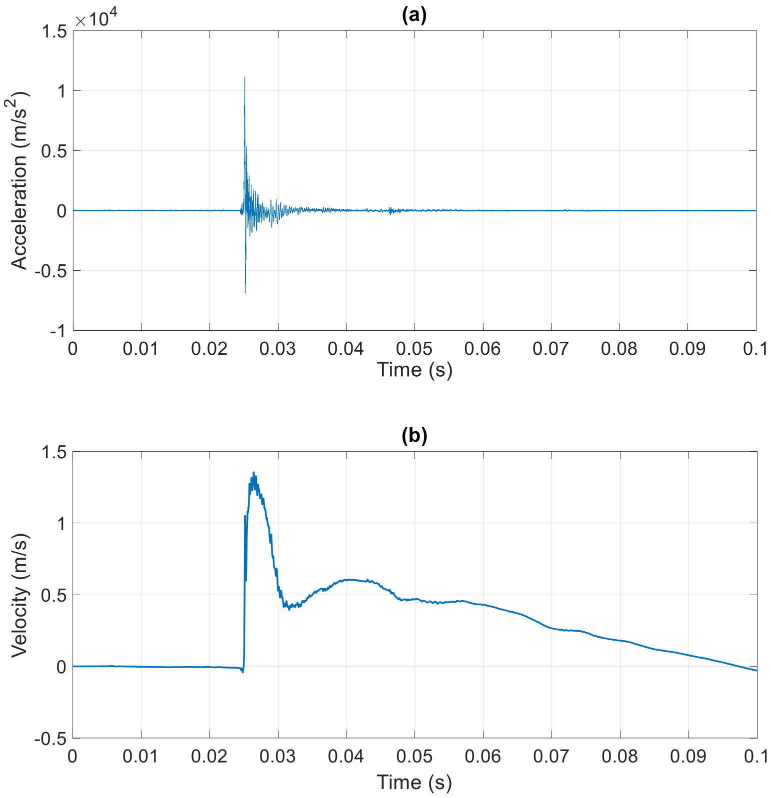

Figure 6-7: (a) Acceleration vs time and (b) Velocity vs time (shot 6 using accelerometer)

6.3.3 Recoil velocity comparison

Figure 6-8 below shows the velocity identified by the HSV and the accelerometer for shot 6 (as shown in Figure 6-4 and Figure 6-7). The graph shows that the velocity data obtained from the accelerometer is not as good as the velocity data obtained from the HSV. This observed difference is due to the oscillation in the measured acceleration signal, which leads to significant integration errors. The same trend was observed for all nine shots. For this reason, the focus is placed on the HSV readings only.

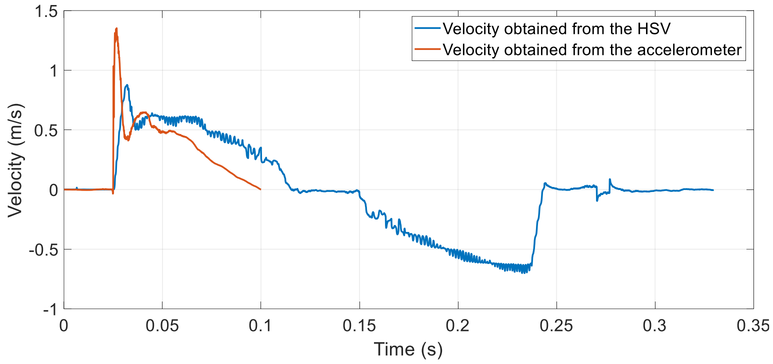

Figure 6-8: Velocity vs time (accelerometer and HSV comparison for shot 6)

6.4 Limitations of the Experimental Data

Some limitations of the experimental data were considered, including:

- Uncertainty regarding acceleration measured data. The acceleration signal appears to have extremely large response magnitudes and periodic time data.

- Uncertainty regarding breech pressure measured data. The first and second shots have inconsistent responses because the pressure transducer was not properly aligned while the other shots show consistent readings.

6.5 Breech Force Verification

The measured MV of the projectile was used to identify the impulse using the change in momentum of the projectile mass to verify the force derived from the pressure. To illustrate this, multiply the measured MV of a projectile of approximately 250 m/s by a projectile mass of approximately 0.234 kg. The resulting impulse should be on the order of 58.5 Ns, which shows that the pressure-derived force is accurate.

Figure 6-9 below shows the force measurements derived from the pressure the impulse from the pressure for shots 5, 6, 8 and 9.

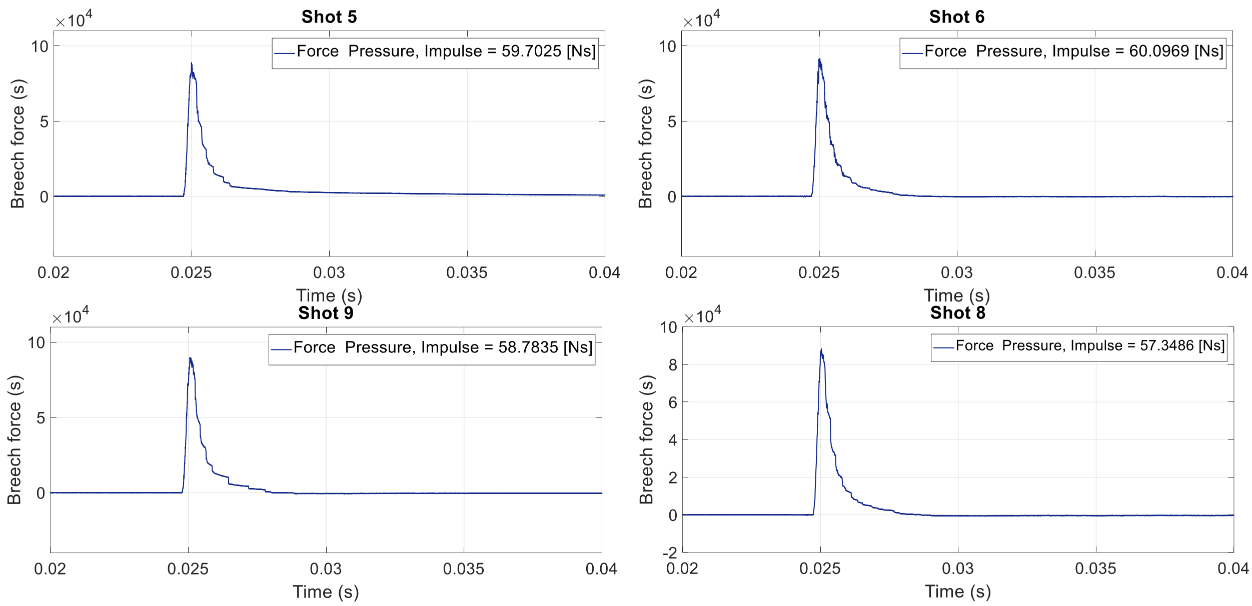

Figure 6-9: Force vs time (derived from pressure)

Table 6-3 summarises the measured data for the MV, the mass of the projectile, the change in momentum and the impulse for each shot. The projectile mass was identified using a digital scale (refer to Appendix B).

Table 6-3: MV, projectile mass, change in momentum and area under the curve (impulse)

Shot number	1	2	3	4	5	6	7	8	9
MV (m/s)	253.83	251.68	251.97	252.39	244.79	252.2	241.68	248.17	250.31
Projectile mass (kg)	0.2343	0.2343	0.2343	0.2341	0.2344	0.2343	0.2341	0.2340	0.2343
Change in momentum (kgm/s)	59.472	58.968	59.036	59.084	57.378	59.090	56.577	58.071	58.647
Impulse (Ns)	70.099	19.418	13.052	69.357	59.702	60.096	56.817	57.348	58.783
Error (%)	16.4	100.9	127.5	15.9	3.9	1.6	0.4	1.2	0.2

The error percentage was determined by calculating the difference between the impulse and the change in momentum. Table 6-3 shows that the error percentage ranges from 0.2% to 16.4% for shots 1, 4, 5, 6, 7, 8 and 9. However, shots 2 and 3 show inconsistency of the impulse. The reason for this inconsistency originates from the lack of accuracy in the pressure measurement because the transducer was not aligned correctly.

6.6 Recoil Velocity Verification

To add more confidence to the HSV readings, the measured projectile MV was used to identify recoil velocity of the proof weapon (or rather recoiling mass) upon muzzle exit of the projectile. This was done by applying a momentum balance between the projectile and recoiling mass. This was evaluated by multiplying the mass of the projectile by its velocity divided by the recoiling mass. The results are presented in Table 6-4.

Table 6-4: Maximum theoretical and measured recoil velocity

Shot number	1	2	3	4	5	6	7	8	9
Maximum recoil velocity (theoretical) (m/s)	0.648	0.643	0.643	0.644	0.625	0.644	0.617	0.633	0.639
Maximum recoil velocity (measured) (m/s)	0.620	0.609	0.608	0.622	0.600	0.605	0.601	0.618	0.629
Error (%)	4.4	5.4	5.5	3.4	4.0	6.2	2.6	2.3	1.5

The error percentage was determined by calculating the difference between the maximum measured recoil velocity and the theoretical recoil velocity values. The error percentage ranges from 1.5 to 6.2%.

6.7 Validation of the Numerical Model

Validation is used to determine the accuracy of a model compared to the real-world situation based on the intended use of that model (AIAA, 1998). This section compares the characterised (Section 5.2.2) and predicated spring stiffness for each shot to validate the recoil simulation program presented in Chapter 4. The simulated and measured data recoil displacement used as the condition for iterating are also presented.

6.7.1 Measured displacement and numerical model

The numerical simulation program introduced in Section 4.4 is used to predict the equivalent spring stiffness of the weapon system using the measured breech force of shot 6 (derived from breech pressure), the displacement of shot 6 and characterised recoiling mass of the weapon system (introduced in Section 5.2.1) as inputs to the model. The numerical model solution is iterated with a change in equivalent spring stiffness while comparing the simulated displacement to the actual measured data for shot 6. By taking the difference between the simulated and measured displacement, the model can identify which spring stiffness shows the smallest comparative error, which means the model converged to that stiffness.

Figure 6-10 shows measured displacement vs time data for shot 6 and simulated displacement with a change in spring stiffness values.

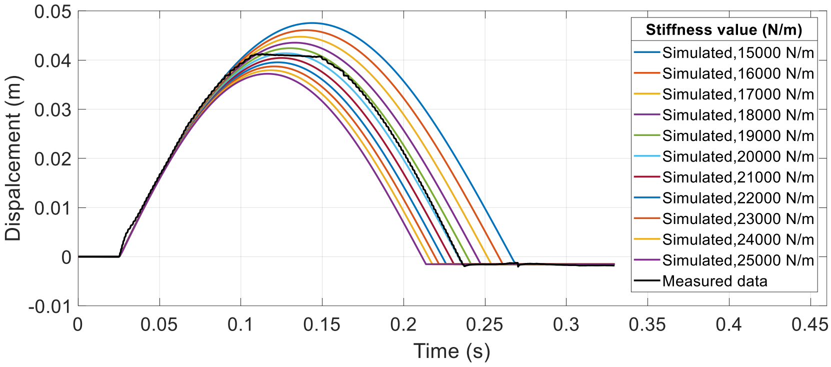

Figure 6-10: Displacement vs time (simulated and actual measured data for shot 6)

As can be seen from Figure 6-10 that the spring stiffness value of the solution that yields the smallest comparative error is 19000 N/m. The solution is then used as a centre coefficient to re-iterate various spring stiffness values until the displacement converges. Figure 6-11 presents the simulated displacement that yields the smallest comparative error to the measured displacement. The predicted spring stiffness value of shot 6 from the model is 19900 N/m.

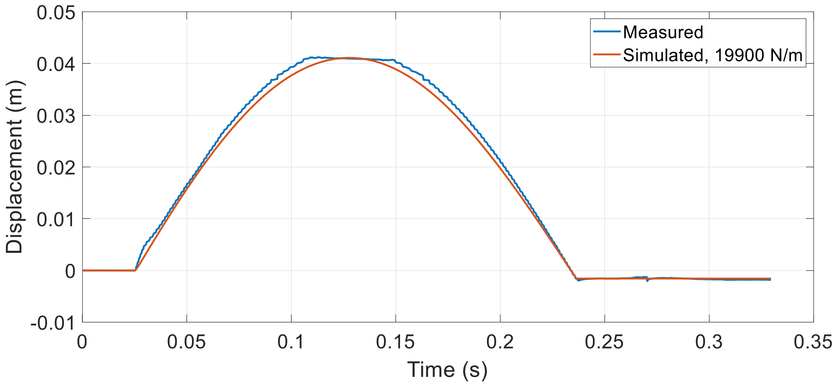

Figure 6-11: Converged displacement vs time (simulated and actual measured data for shot 6)

In Figure 6-11 above, the recoil simulation model slightly over-predicts the magnitude of the measured displacement curve at the first 0.12 seconds. The average overall error of the curve is approximately 0.0051%, and the maximum recoil displacements for the numerical simulation model and the actual measurement are approximately 0.042 m and 0.041 m, respectively.

The same process to predict the spring stiffness value of shot 6 was applied for shots 5, 7, 8 and 9. Figure 6-12 below presents the simulated displacement that yields the smallest comparative error to the measured displacement of each individual shot. Therefore, the predicted spring stiffness values of shots 5, 7, 8 and 9 from the model are 21100 N/m, 19300 N/m 19500 N/m and 19700 N/m respectively.

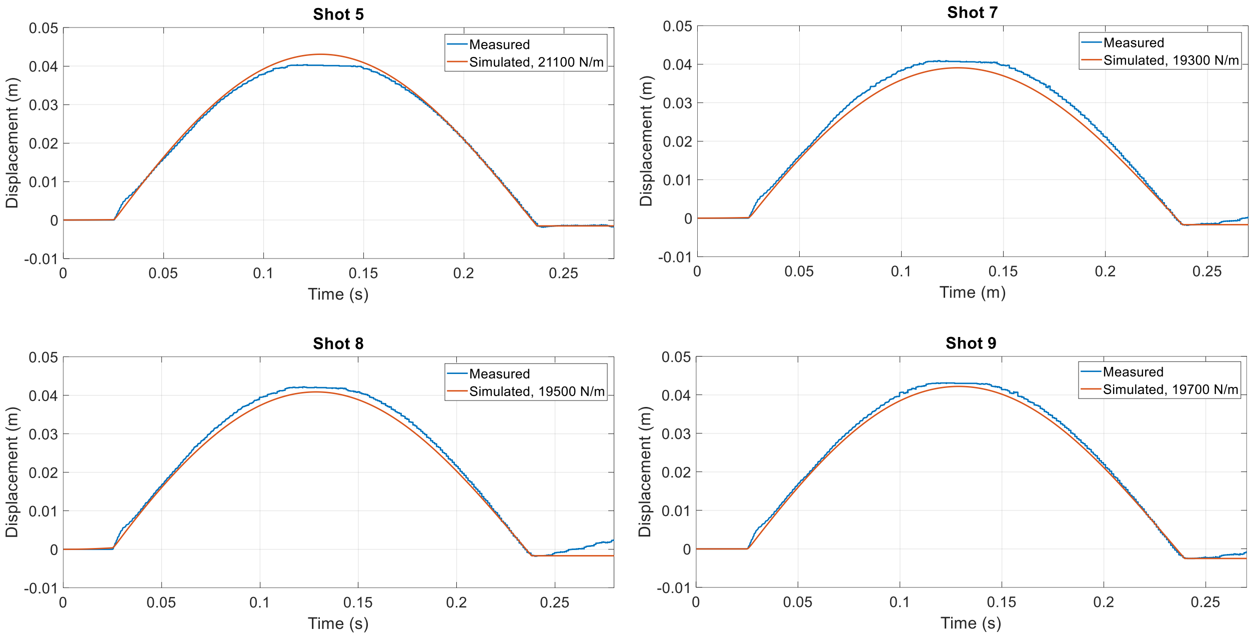

Figure 6-12: Displacement vs time (simulated and actual measured data for shots 1, 5, 7 and 8)

As can be seen in Figure 6-12, slight differences exist between the measured and simulated displacement amplitudes for shots 5, 7, 8 and 9. To illustrate this, the impulse (the area under the breech force curve) was calculated using the trapezoid method for each of the shots (refer to Table 6-3). The differences in impulse values affect the simulated displacement amplitudes. The reason for the inconsistency of the force impulse originates from the lack of accuracy in the pressure measurement. Measuring pressures of high amplitude and short durations is always complex.

6.7.2 Model and measurement spring stiffness comparison

Table 6-5 compares the spring stiffness value of the equivalent spring stiffness predicated by the recoil simulation program and the characterised equivalent spring stiffness of the weapon system (determined in Section 5.2.2).

Table 6-5: Predicted vs characterised equivalent spring stiffness

Shot number	1	2	3	4	5	6	7	8	9
Characterised spring stiffness (N/m)	19372	19372	19372	19372	19372	19372	19372	19372	19372
Predicted spring stiffness (N/m)	20000	20500	21400	21000	21100	20300	19300	19500	19700
Error (%)	3.1	5.5	9.4	7.7	8.1	4.6	0.3	0.6	1.6

Table 6-5 demonstrates that the predicted spring stiffness of the numerical model program correlates well to the experimentally characterised spring stiffness. The error percentage ranges between 0.3% to 9.4% for the nine shots. At this stage, the numerical simulation program is considered to be validated.

To conclude, after the stiffness of the recoiling spring is correctly determined by the followed procedure, the spring stiffness can be used in internal ballistic simulation models to reduce the uncertainty.

6.8 Summary

In this chapter, all results of the experimental tests were provided and discussed. The data analysis techniques were discussed in detail. The comparison between predicted spring stiffness (from the simulation program) and characterised spring stiffness indicated an acceptable correlation, which validates the process used to derive the simulation program.

CHAPTER 7 - CONCLUSION

7.1 Research Overview

The first chapter provided an introduction into the relevant aspects of internal ballistics and recoil, which forms the basis of this research. The problem statement of this research was considering the effect that recoil has on the ballistic system. The research objectives were stated. The research aimed to develop a framework to characterise the recoil system. Then, these characteristics can be used in the internal ballistic modelling. The limitations were stated and the contributions of the study were outlined.

The second chapter provided the concepts of the internal ballistic modelling. It also explained the role of the recoil, functions of the recoil system and components of recoil mechanism. Furthermore, it highlighted vibration, resistive recoil force model, and impulse and momentum.

The third chapter introduced the weapon system involved in the investigation. It also highlighted the numerical model and the analytical model of the recoiling mechanism.

Chapter four explained the implementation of the fourth-order Runge-Kutta (numerical method). In addition to that, it described the implementation of the analytical model. It also conducted a verification analysis.

The fifth chapter defined the characterisation of the elements of the weapon system. It also discussed the test set-up as well as the followed methodologies to obtain the measured data. It also explained the data processing.

Chapter six discussed the gathered results during the firing trails of the 40mm weapon system. It also analysed the gathered data. Furthermore, it compared the two stiffness values of the recoil spring, which were obtained by the simulation model and experiment.

7.2 Conclusion

The objective of this research was to develop a framework to characterise a recoil system. Then throughout the framework, the generated characteristics of the recoil system can be used in internal ballistic modelling.

Throughout this research, the framework was proposed and developed. The generated output of the framework was the spring stiffness of the 40mm weapon system. Then, the value of spring stiffness was validated by conducting a physical test on the recoiling spring using the deflection test. Based on that finding, the framework was verified.

The developed framework to characterise a recoil system is applicable to any (Springs Only) recoil system without disassembling the recoiling component. Some recoiling systems are complicated and hard to disassembled, which give the developed framework an advantage.

The recoil spring stiffness can be used in the internal ballistic simulation programme to improve the accuracy of the programme and reduce the uncertainties.

7.3 Recommendation

A two-dimensional iterative process must be used to model a weapon system with damping. Using the recoil force as an additional parameter to obtain extra input data for the model to accelerate convergence is recommended.

7.4 Future Work

- The method / process used in this research can be applied and tested on other weapon systems, which are approximated as a SDOF with spring stiffness only (25 mm, 30 mm, 76 mm, 105 mm, etc.), and

- Damping can be included into the method / process which will require expansion of the process and program.

BIBLIOGRAPHY

Agrawal, J. P. (2010). *High Energy Materials: Propellants, Explosives and Pyrotechnics.* Wiley-VCH Verlag GmbH & Co.KGaA.

AIAA. (1998). *Guide for the verification and validation of computational fluid dynamics simulations.* Reston, VA: American Institute of Aeronautics and Astronautics, G-077.

AMC. (1964). *Research and development of materiel: engineering design handbook: guns series, guns general.* Washington: U.S. Government Printing Office: AMC Pamphlet, (pp 706-250).

Bhave, S. (2010). *Mechanical vibrations: theory and practice.* New Delhi: Dorling Kindersley.

Brown, D. (2005). Chapter 16 Tracker. In C. Wolfgang , *Open Source Physics: A User's Guide with Examples* (pp. 337-365). Author.

Carlucci, D. E., & Jacobson, S. S. (2013). *Ballistics : Theory and design of guns and ammunition* (2nd ed.). Boca Raton: CRC Press, Taylor & Francis Group.

DND Canada. (1992, 06 01). Field Artillery. *Ballistics and Ammunition, Volume 6*, p. 286.

DOD. (1988). *Military Handbook Recoil Systems DOD-HDBK-778.* Washington, DC 20301: Author.

Gander, T. J. (2002). *Jane's infantry weapons, 2002-2003.* (28, ed.) Coulsdon, UK : Jane's Information Group.

Hoffman, J. D. (1992). *Numerical methods for engineers and scientists.* New York: Marcel Dekker, Inc.

Horn, F., & Boutteville, S. V. (1982). Gun; Gun Mechanics. In G. R, *Rheinmetall Handbook on Weaponry* (pp. 295-495). düsseldorf: Rheinmetall GmbH.

Paz, M., & Leigh, W. (2004). *Structural Dynamics : Theory and Computation* (5 ed., Vol. 1). Kluwer Academic Publishers.

Piersol, A. G., & Paez, T. L. (2002). *Harris' shock and vibration handbook* (5 ed.). New York: McGraw-Hill.

Rao, S. S. (2011). *Mechanical vibrations* (5 ed.). Upper Saddle River, NJ, United States: Prentice Hall.

Schabort, V. (2016). *RDM Internal Ballistic.* Somerset West: RDM.

STANAG-4367. (2000). NATO - Thermodynamic Interior Ballistic Model with Global Parameters.

USMA. (1980). The twelfth in a series of army science conference. *Proceedings of the Army Science Conference. 4*, p. 504. West Point, New York: Office of the Deputy Chief of Staff for Research, Development, and Acquisition.

APPENDIX A

A.1 Numerical model program (MATLAB code):

```
clear all;
clc()
close all;

leg=[];
n_k=1;
figure

global excit m k SR

%Load sensor data for shot 6
dat = csvread('Shot_File_name1.csv'.csv',3);
% dat=magic(206);
%Use column 1 to 3 of loaded data
%Column 1 represents the measured pressure
%Column 2 is not used
%Column 3 represents the measured trigger of the HSV
y = dat(4:length(dat(:,1)),1:3);
SR = 5E-07 ; %Sample rate used for measured sensor data
n = length(y(:,1)) ; %Length of the measured pressure data set, will be used
to generate time vector
t = zeros(); %Define time vector for sensor data

%Populate time vector with steps of sample rates
for i = 2:n
    t(i,1) = t(i-1,1) + SR;
end

%Convert measured pressure data to breech force with the definition F = P.A
A = (pi/4)*(41^2) ; %Breech area of the gun
ya(:,1) = y(:,1)*A ;   %Measured pressure data set times the breech area

%Identify time stamp of HSV trigger
index = find(y(:,3)>50) ;   %First spike in data set used to trigger HSV
t_zero = t(index(1,1),1);    %Time stamp of the first spike in HSV trigger

%Filter breech force data with moving average filter
window = 100  ;  %Moving average filter - window size
b = (1/window)*ones(1,window) ;  %Define filter function
yf = filter(b, 1, ya(:,1));  %Apply filter

%Generate a time and excitation (similar to the breech force) vector that aligns
with HSV data
time(1,1) = 0 ;  %Define first data point of time vector for HSV
excite = zeros(); %Define excitation vector, to be later used for numerical
model
excite (1,1) = ya(1,1) ;   %Define first data point of excitation vector
%Populate time and excitation vectors
for i = 2:n
    time(1,i) = time(1,i-1) + SR;
    excite(1,i) = yf(i,1);
end
```

```
%Increase time and excitation vector to match the length of the HSV data set
r = (1.5 - time(1,i))/SR;
for l = i+1:r
    time(1,l) = time(1,l-1) + SR;
    excite(1,l) = 0;
end

%Load HSV data for shot 6
dathsv = csvread('Shot_File_name2.csv'.csv');

%Use column 1 to 2 of loaded data
%Column 1 represents the time vector for the HSV data set
%Column 2 represents the tracked displacement for the HSV data set
z = dathsv(1:length(dathsv(:,1)),1:2);

%Define the "zero" point for the displacement data set
dc = 0;
for i=1:100
    dc = dc+z(i,2);
end
dc = dc/100;

z(:,2) = (z(:,2) - dc)/1000 ;%Zero data set by decoupling the DC-offset and
convert displacement to meters
z(:,1) = z(:,1) - (300*(1/10000)) + t_zero;  %Use the time stamp of the first
HSV trigger earlier defined and correct the HSV time vector
zend = z(length(z(:,1)),1);   %This is later used in the numerical model to
define iteration steps


%Filter displacement data with moving average filter
for ii =1:size(shot1,2)
    AvrageCoef          = ones(1, DataPoint1)/DataPoint1;
    shotFilt1(:,ii)       = filter(AvrageCoef, 1,shot1(:,ii));
end

%Numerical model properties
m = 91.11; %Total recoiling mass

for k = 15000:1000:25000 %Spring stiffness

%Boundary conditions & Vector definitions
step = 1e-4; %Step size in time (seconds) for the integration loop
x = zeros(); %Numerical model displacement
v = zeros(); %Numerical model velocity
tp = zeros();    %Numerical model time vector
tim = 0; %Initial condition of time

%4th Order Runge Kutta - Loop
for i=1:round(zend/step)
    k11 = step*f1(x(1,i),v(1,i),tp(1,i));
    k21 = step*f2(x(1,i),v(1,i),tp(1,i));
    k12 = step*f1(x(1,i)+0.5*k11,v(1,i)+0.5*k21,tp(1,i)+0.5*step);
    k22 = step*f2(x(1,i)+0.5*k11,v(1,i)+0.5*k21,tp(1,i)+0.5*step);
    k13 = step*f1(x(1,i)+0.5*k12,v(1,i)+0.5*k22,tp(1,i)+0.5*step);
    k23 = step*f2(x(1,i)+0.5*k12,v(1,i)+0.5*k22,tp(1,i)+0.5*step);
    k14 = step*f1(x(1,i)+k13,v(1,i)+k23,tp(1,i)+step);
    k24 = step*f2(x(1,i)+k13,v(1,i)+k23,tp(1,i)+step);
```

```
    x(1,i+1) = x(1,i) + (k11+2*k12+2*k13+k14)/6;
    v(1,i+1) = v(1,i) + (k21+2*k22+2*k23+k24)/6;
    tp(1,i+1) = tp(1,i)+step;

end

%Plot
plot (subplot(3,1,1),tp,x) %Displacement plot
hold on
plot (subplot(3,1,2),tp,v) %Velocity plot
hold on
leg =[leg ; num2str(k)]; % Legend recorder
legend(leg)

% Average Error
K(n_k)                  = k;
X(n_k,:)                = x(1,:);
V(n_k,:)                = v(1,:);
Sq_Error(:,n_k)         =(rot90(x,3)+[z(:,2)]);
Sum(n_k)                = sum(Sq_Error(:,n_k));
ErrorAve(n_k)           = abs(Sum(n_k)/length(x));
n_k                     = n_k+1;

end

[AverageError,Index]               = min(ErrorAve);
disp(' Spring Coeffeciant index');
disp(Index);
disp(' Spring Coeffeciant is equal to');
disp(K(Index));
disp(' Error is equal to');
disp(AverageError);
plot (subplot(3,1,1),z(:,1),-z(:,2),'color',[0 0 0]) %Reference plot
plot (subplot(3,1,3),z(:,1),-z(:,2),'color',[0 0 0]) %Reference plot
hold on;
plot (subplot(3,1,3),tp,X(Index,:),'color',[0 0 0]) %Reference plot
hold on;
plot (subplot(3,1,2),time1,y1,'color',[0 0 0]) %Reference plot
hold off

plot(z(:,1),-z(:,2));
hold on
plot (tp,x);
hold off

plot (z(:,1),-z(:,2),'color',[0 0 0]) %Reference plot
hold on;
plot (tp,X(Index,:),'color',[0 0 0]) %Reference plot
hold on;
figure
plot(ErrorAve)
xlabel('Number of iteration')
ylabel('Avrage Error')

%Differential Equations Function Model
%Two first order differential equations
%1. dx1/dt = x2(t)
function [dx1dt] = f1(dis,vel,tim)
    dx1dt = vel;
```

```
end

%2. dx2/dt = f(t) - k*x1(t)
function [dx2dt] = f2(dis,vel,tim)
global excite m k SR

    if tim == 0 %then
        dx2dt = (excite(1,1))/m -(k/m)*dis;
    else
        dx2dt = (excite(1,round(tim/SR)))/m - (k/m)*dis;%
    end
end
```

A.2 Analytical model program:

```
clear all;
clc;
m        = 90; %Mass
k        = 19000; %spring Stiffness
F0       = 90000; %Force acts on the mass [N]
wn       = (k/m)^0.5; %The natural frequency of the system
w        = 10; %Frequency

if (w/wn) < 1
    X    = (F0/k)/(1-(w/wn)^2);    %Case 1. % X is an constant that denotes the
maximum amplitude of xp(t)
else
    X    = (F0/k)/((w/wn)^2 - 1); %Case 2. X is an constant that denotes the
maximum amplitude of xp(t)
end
%initial conditions
x0       = 0.0;
x0_dot   = 0.0;

t        = 0:0.001:4; %Time
if (w/wn) < 1

    xp   = X*cos(w*t);                          %Case 1. When the Eq. positive
(displacement)
    [~,vp] = ode23(@(t,vp)X*cos(w*t),t,0); %Case 1. 1st derivative (velocity)
else
    xp   = -X*cos(w*t);                         %Case 2. When the Eq. negative
(displacement)
    [~,vp]= ode23(@(t,vp)-X*cos(w*t),t,0); %Case 2. 1st derivative (velocity)
end
    F   = F0*cos(w*t);                    %Harmonic response (Excitation force)
%Substituting the analytical solution above into the governing differential
equation

x=(x0-F0/(k-m*w^2))*cos(wn*t)+(x0_dot/wn)*sin(wn*t)+(F0/(k-m*w^2))*cos(w*t);


%Plotting
%Dispacement vs. Time
figure(1);
plot (t,xp);
xlabel ('t');
ylabel ('x(t)');
```

```
%Excitaion Force vs. Time
figure(2);
plot (t,F);
xlabel ('t');
ylabel ('F(t)');
```

APPENDIX B

B.1 Characterisation of system mass

The recoiling mass was identified by adding the mass of the parts to the recoiling mass of the test setup. The Figure 1 below shows the complete recoiling mass of the test setup.

Figure 1: Mass of recoiling parts

B.2 Characterisation of system stiffness

A load cell (BM U2A) and a displacement transducer (HBM W20) were connected to a bridge amplifier/data acquisition system. A force was then applied onto the platform while the displacement and force were measured simultaneously. The Figure 2 below illustrates the setup.

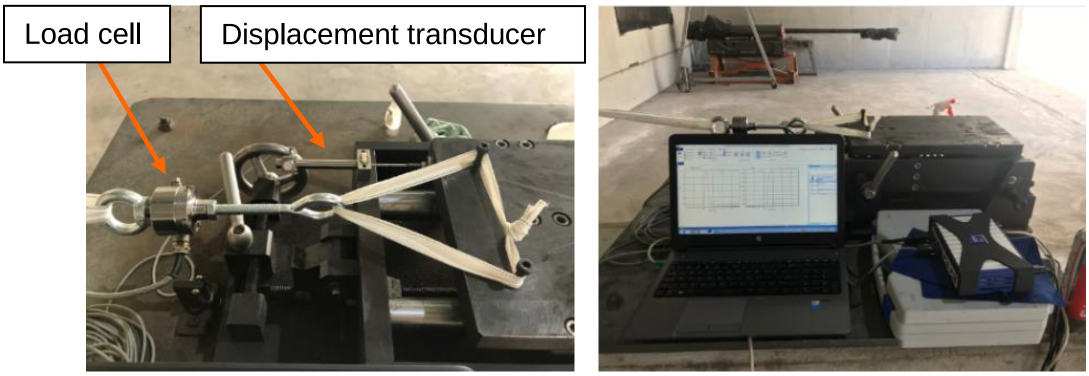

Figure 2: Test setup for measuring force and displacement

B.3 Test setup break down

B.3.1 Piezoelectric pressure transducer orientation

The pressure transducer was installed in the barrel as shown in Figure 3

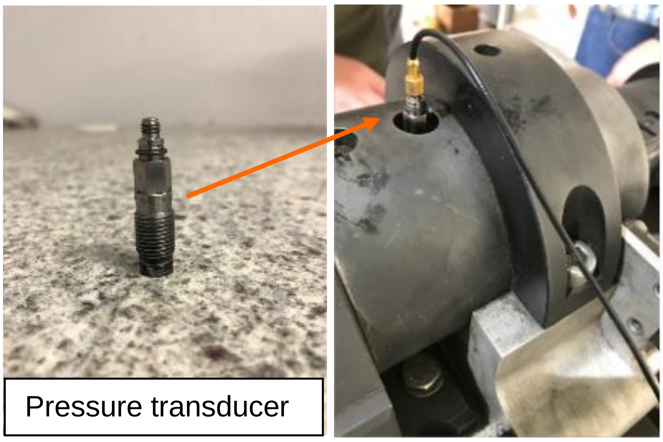

Figure 3: Installation of the piezoelectric pressure transducer

B.3.2 High-speed video

The Figure 4 shows how the high-speed video was spaced perpendicular to the weapon firing

Figure 4: HSV

B.3.3 Accelerometer

The accelerometer was glued to the recoil plate as can be seen in the Figure 5.

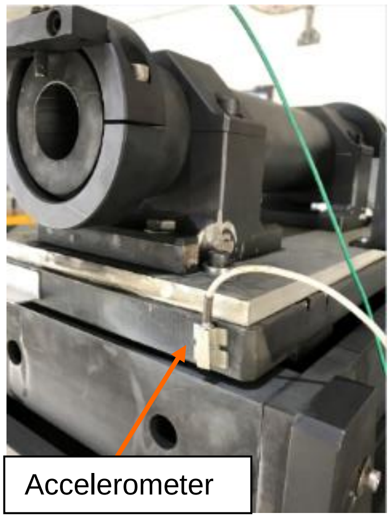

Figure 5: Accelerometer

B.3.4 Light gate device

The light gate device was spaced 4 meters from the muzzle of the proof gun as can be seen in the Figure 6.

Figure 6: Light gate device